The roles of electronic exchange and correlation in charge-transfer-to-solvent dynamics: Many-electron nonadiabatic mixed quantum/classical simulations of photoexcited sodium anions in the condensed phase

William J. Glover, Ross E. Larsen, and Benjamin J. Schwartz[a)]
Department of Chemistry and Biochemistry, University of California, Los Angeles,
Los Angeles, California 90095-1569, USA

The charge-transfer-to-solvent (CTTS) reactions of solvated atomic anions serve as ideal models for studying the dynamics of electron transfer: The fact that atomic anions have no internal degrees of freedom provides one of the most direct routes to understanding how the motions of solvent molecules influence charge transfer, and the relative simplicity of atomic electronic structure allows for direct contact between theory and experiment. To date, molecular dynamics simulations of the CTTS process have relied on a single-electron description of the atomic anion—only the electron involved in the charge transfer has been treated quantum mechanically, and the electronic structure of the atomic solute has been treated via pseudopotentials. In this paper, we examine the severity of approximating the electronic structure of CTTS anions with a one-electron model and address the role of electronic exchange and correlation in both CTTS electronic structure and dynamics. To do this, we perform many-electron mixed quantum/classical molecular dynamics simulations of the ground- and excited-state properties of the aqueous sodium anion (sodide). We treat both of the sodide valence electrons quantum mechanically and solve the Schrödinger equation using configuration interaction with singles and doubles (CISD), which provides an exact solution for two electrons. We find that our multielectron simulations give excellent general agreement with experimental results on the CTTS spectroscopy and dynamics of sodide in related solvents. We also compare the results of our multielectron simulations to those from one-electron simulations on the same system [C. J. Smallwood *et al.*, J. Chem. Phys. **119**, 11263 (2003)] and find substantial differences in the equilibrium CTTS properties and the nonadiabatic relaxation dynamics of one- and two-electron aqueous sodide. For example, the one-electron model substantially underpredicts the size of sodide, which in turn results in a dramatically different solvation structure around the ion. The one-electron model also misses the existence of an entire manifold of bound CTTS excited states and predicts an absorption spectrum that is blueshifted from that in the two-electron model by over 2 eV. Even the use of a quantum mechanics/molecular mechanics (QM/MM)-like approach, where we calculated the electronic structure with our CISD method using solvent configurations generated from the one-electron simulations, still produced an absorption spectrum that was shifted ~1 eV to the blue. In addition, we find that the two-electron model sodide anion is very polarizable: The instantaneous dipole induced by local fluctuating electric fields in the solvent reaches values over 14 D. This large polarizability is driven by an unusual solvation motif in which the solvent pushes the valence electron density far enough to expose the sodium cation core, a situation that cannot be captured by one-electron models that employ a neutral atomic core. Following excitation to one of the bound CTTS excited states, we find that one of the two sodide valence electrons is detached, forming a sodium atom:solvated electron contact pair. Surprisingly, the CTTS relaxation dynamics are qualitatively similar in both the one- and two-electron simulations, a result we attribute to the fact that the one-electron model does correctly describe the symmetry of the important CTTS excited states. The excited-state lifetime of the one-electron model, however, is over three times longer than that in the two-electron model, and the detachment dynamics in the two-electron model is correlated with the presence of solvent molecules that directly solvate the cationic atomic core. Thus, our results make it clear that a proper treatment of anion electron structure that accounts for electronic exchange and correlation is crucial to understanding CTTS electronic structure and dynamics. © *2008 American Institute of Physics.*
[DOI: 10.1063/1.2996350]

[a)]Author to whom correspondence should be addressed. Electronic mail: schwartz@chem.ucla.edu.

I. INTRODUCTION

In the gas phase, atomic anions do not have bound electronic excited states. By contrast, in solution, many of these anions show intense absorption bands in the ultraviolet-visible range, indicating the appearance of bound electronic excited states that are associated with the presence of the solvent. Historically, these excited states were termed charge-transfer-to-solvent (CTTS) states with the expectation that they were intimately associated with the solvent molecules; indeed, the absorption bands are very sensitive to the choice of solvent, temperature, and the presence of cosolutes or cosolvents.[1–3] However, modern work has found that these excited CTTS states are actually fairly localized in the solvent cavity that contains the anion, so that the acronym CTTS is somewhat of a misnomer.[4] These solvent-supported CTTS states are only quasibound, and excitation to them results in the production of a solvated electron that is free from the neutral atomic core,[2,5,6] a process referred to as a CTTS reaction. CTTS systems thus represent simple models of charge-transfer reactions in which all of the dynamics are driven by motions of the solvent or by solute translations since atomic anions have no internal degrees of freedom. This is why these systems have been the subject of many ultrafast pump-probe studies seeking to understand the solvent dynamics associated with charge transfer.[5–38]

Although ultrafast spectroscopic studies have brought our understanding of these CTTS reactions a long way (for an excellent review see Ref. 16), transient spectroscopy alone cannot provide molecular detail about what the solvent does during the course of a CTTS reaction, so computer simulations are necessary to build a complete picture of the reactivity in these model systems. In order to accurately simulate these reactions, quantum mechanics must be invoked since the solvated electron product of a CTTS reaction is a highly quantum object. Using quantum mechanics to treat all the particles involved in a CTTS reaction is prohibitively computationally expensive, so molecular dynamics (MD) simulations of CTTS reactions usually adopt a mixed quantum/classical (MQC) approach whereby only the electron involved in the charge transfer is treated quantum mechanically and the other particles are treated classically. The first MQC MD simulations of a CTTS reaction were performed by Sheu and Rossky,[4,39–41] who studied the electron photodetachment dynamics of aqueous iodide. These simulations showed that some of the original ultrafast experiments on iodide in water[7] involved direct multiphoton excitation to the water conduction band rather than CTTS excitation.[8] Staib and Borgis[42–45] carried out similar simulations of the related aqueous chloride system and studied the potential of mean force between the detached electron and its Cl atom partner. In addition to the halides, Smallwood et al.[46] studied the CTTS dynamics of the aqueous sodium anion (sodide), a model system constructed to explore the role of electronic symmetry in the photodetachment dynamics of aqueous anions. Although it cannot be prepared experimentally, Smallwood et al.[46] chose to explore this model system for three reasons. First, sodide's CTTS excited states are expected to be p-like, whereas the halide CTTS states are predominantly

s-like,[47] providing direct means to investigate how electronic symmetry affects CTTS dynamics. Second, the aqueous sodium anion system is computationally related to the well-studied hydrated electron,[48,49] allowing the investigation of the role of an attractive nucleus in electronic relaxation processes in water. Finally, there have been numerous ultrafast experimental studies of the CTTS dynamics of sodide (although in solvents other than water), providing a means to make indirect contact with experiment.[18–30,34–36]

An important approximation used in all of the MQC MD simulations of CTTS dynamics performed to date[4,39–46] is to treat only one of the solute anion's valence electrons quantum mechanically. In these studies, the interaction of this quantum mechanical electron with all of the other electrons (on both the solute and solvent) was described via pseudopotentials, a choice that was necessary to make these calculations computationally feasible. However, the use of pseudopotentials for describing halide and alkalide electronic structure leaves room for significant error since the basic assumption of pseudopotential theory is that the core electrons (those treated via pseudopotentials) are chemically inactive and that their properties remain independent of the state of the valence electron(s) (those treated explicitly quantum mechanically).[50,51] Describing sodide as an effective one-electron system, however, means treating one of the two equivalent 3s electrons with a pseudopotential and the other explicitly, which is clearly a gross approximation. A one-electron description of the halides is based on a similarly drastic approximation since five out of the six equivalent p valence electrons are treated implicitly and one is not. To investigate the severity of this approximation for iodide, Bradforth and Jungwirth[47] performed many-electron calculations of the CTTS electronic structure of aqueous iodide using solvent configurations extracted from a classical MD trajectory. These authors found that their many-electron treatment produced a qualitatively different electronic structure than that found by Sheu and Rossky,[4,39–41] who had used a one-electron halide model. Sheu and Rossky[41] found that the (one-electron) aqueous iodide CTTS absorption band arose from a superposition of many transitions between a single iodide ground-state p-electron and six CTTS excited states with mixed s- and d-character. In contrast, Bradforth and Jungwirth[47] found that the (many-electron) iodide absorption spectrum consisted of only three transitions, which arose from the excitation of an electron from one of the three iodide ground-state valence p-orbitals to a single CTTS excited state of mixed s- and p-character. The many-electron calculations of Bradforth and Jungwirth provided much better agreement with the experimental absorption spectrum, and their assignment that excitation of this band produces only a single CTTS excited state is supported by the experimental observation that the detachment and recombination dynamics of photoexcited aqueous iodide are invariant as the excitation wavelength is tuned across the CTTS band.[13] Thus, it is apparent that the use of one-electron models in quantum MD simulations of CTTS reactions can predict the wrong number and incorrect symmetry of the bound CTTS excited states, putting any dynamics calculated with these simulations into question.

Our goal in this paper is to understand how the calculated quantum dynamics of CTTS reactions are modified when one goes beyond a one-electron picture and uses an appropriate many-electron model to describe the anion. Bradforth and Jungwirth[47] were unable to explore such dynamics for aqueous iodide since the nuclear configurations in their calculations were generated from a classical trajectory that could not respond to changes in the quantum wave function upon CTTS excitation. In this paper, we revisit the quantum dynamics of the simpler (from a computational perspective) aqueous sodide system, using a many-electron description to explore the effects of correlation and exchange between the sodide valence electrons on both CTTS electronic structure and dynamics. Even though aqueous sodide is not experimentally realizable, studying this system allows us to directly compare our new multielectron simulations with the previous one-electron work[46] and thus isolate how changes in the quantum treatment of the valence electrons affect the calculated electronic structure and photodetachment dynamics. These simulations will also help us to understand alkali anion CTTS dynamics in the limit of a highly polar solvent, providing a connection to the increasing number of ultrafast pump-probe experiments on this anion.[18–30,34–36] Finally, our choice to study the aqueous sodide system also allows us to make connection with recent simulations of the hydrated dielectron (two excess electrons solvated in a single water cavity) by Larsen and Schwartz[52–56] because aqueous sodide may be envisioned as a hydrated dielectron attached to a positive sodium ion Na^+. This provides us a means to explore how the presence of a cationic nucleus alters the relaxation dynamics of the dielectron, so that we can learn something general about the dynamic solvation of aqueous anions.

The rest of this paper is organized as follows. In Sec. II, we discuss the computational methods used in our nonadiabatic, many-electron MQC MD simulations; in particular, we treat the two sodide valence electrons using a version of configuration interaction with singles and doubles (CISD), which, in principle, gives an exact treatment of these two electrons.[52] In Sec. III we compare the equilibrium properties of aqueous sodide calculated with our CISD method to those obtained with the previous one-electron model.[46] We find both quantitative and qualitative differences in the equilibrium properties of sodide as calculated in the two models. In particular, the one-electron model grossly underpredicts the size of the aqueous sodide ion, leading to substantial differences in both the solvent structure around sodide and the CTTS absorption spectrum. In Sec. IV, we examine the nonequilibrium relaxation dynamics of aqueous sodide following excitation to the lowest CTTS state. We find that the solvent response to excited sodide causes an electron to be ejected from the sodium core to form a neutral sodium atom:solvated electron contact pair. Once the system makes a nonadiabatic transition to the ground state, in some trajectories one of the electrons detaches completely from the core, while in the remaining trajectories there is a rapid recombination to reform the sodide ion; this behavior is qualitatively similar to that observed in the previous one-electron simulations of sodide.[46] We conclude in Sec. V by noting that the

similarity in relaxation pathways for photoexcited sodide in both the one-electron model and two-electron model suggests that it is the similarity in electronic symmetry of the ion in both models that is the important factor in determining the nonequilibrium relaxation pathways. Thus, even though the one-electron model makes large quantitative errors in many of sodide's properties, the one-electron model does get the basic electronic symmetry of the ion correct and thus can qualitatively predict the types of nonequilibrium relaxation we see in the more accurate two-electron model. Finally, we include Appendixes A and B detailing the construction of our sodium pseudopotential and our spherical harmonic analysis of the CI wave functions.

II. MODEL AND COMPUTATIONAL DETAILS

To facilitate comparison between the results of our two-electron simulations of aqueous sodide (hereafter referred to as 2EM), the previous one-electron simulations on sodide of Smallwood *et al.*[46] (hereafter referred to as 1EM) and also the dielectron simulations of Larsen and Schwartz,[52] we have kept the details of our simulation method as close as possible to these previous simulations. We therefore keep discussion of our simulation methods relatively brief, but pay particular attention to differences between our simulation method and those in previous work.[46,52] Our 2EM system consisted of 1600 classical water molecules and a single Na^- solute represented by a classical Na^+ core plus two fully quantum mechanical valence electrons. The simulation box was cubic with side of 36.34 Å to yield a water density of 0.9970 g cm^{-3}; we note that our simulation box is significantly larger than those used in Refs. 46 and 52, which we found was necessary to prevent finite-size effects on the 2EM solvent structure. We treated the water intra- and intermolecular interactions with the classical flexible single point charge (SPC-flex) potential[57] and represented the water-sodium cation interactions as a sum of Lennard-Jones and Coulombic terms using the parameters given by Balbuena *et al.*[58] We accounted for the electron-solvent and electron-sodium cation interactions with pairwise-additive pseudopotentials that are described in more detail in Sec. II B. Our method for nonadiabatic propagation of the MQC 2EM system is described in Sec. II A, and the quantum chemistry methods we use to solve the Schrödinger equation for the quantum particles are described in Sec. II C. Our simulations employed minimum-image periodic boundary conditions and all interactions were smoothly tapered to zero at 16 Å over a 2 Å range with a group-based cutoff.[59,60]

A. MQC dynamics propagation

For the 2EM simulations of equilibrium ground-state sodide that are discussed in Sec. III, the fact that the energy gap between ground and first excited states is large relative to the fluctuations in these energies allowed us to make use of the adiabatic approximation. In this case, we solved for the adiabatic states of the two quantum electrons at every MD time step using our CISD method, which is described in Sec. II C. The forces on the classical particles due to the quantum electrons were evaluated using the Hellman–Feynman theorem,

$$\boldsymbol{F}_i^q = -\langle \Psi | \boldsymbol{\nabla}_{\boldsymbol{R}_i} \hat{V} | \Psi \rangle, \tag{1}$$

where $\boldsymbol{F}_i^q$ is the quantum force on classical particle i, which is at coordinate $\boldsymbol{R}_i$, $\hat{V}$ is the potential energy operator representing the interaction between classical and quantum particles, and Ψ is the full two-particle wave function. The classical particles' trajectories were propagated using this force plus those from the classical-classical interactions with the velocity-Verlet algorithm[61] with a time step of 1.0 fs. The simulation was performed in the microcanonical ensemble and the average temperature was 300 ± 2.8 K. After equilibrating our 2EM system starting from a configuration taken from the previous 1EM simulations,[46] we ran a 200 ps adiabatic ground-state trajectory. As was done in the previous simulations of hydrated dielectrons,[52] we found it necessary to rescale particle velocities every 10 ps to remove a slow drift in the total energy of our system. This drift results from small errors in the quantum force calculated via Eq. (1) due to using a product basis of only the lowest single-electron states rather than a complete basis involving all possible excited single-electron states.[62] The drift was found to be no worse than 0.06% of the total energy after 10 ps, which is less than the rms fluctuations in energy due to the velocity-Verlet integrator.

For the nonequilibrium excited-state simulations of sodide discussed in Sec. IV, the fact that the energy gaps between excited states are small relative to the energy fluctuations leads to a breakdown of the adiabatic approximation. To account for nonadiabatic effects, we used the mean-field-with-surface-hopping (MF/SH) algorithm of Prezhdo and Rossky,[63] which was also used in the previous 1EM (Ref. 46) and dielectron simulations.[52] This algorithm propagates the quantum electronic state as a linear combination of the adiabatic states (in our simulations we used the lowest ten adiabatic states) and provides a method to mimic quantum decoherence as the occasional collapse of the mean-field superposition state into one of the adiabatic states; these collapses can be either "surface-hopping" or "mean-field rescaling" events. For further details of the MF/SH algorithm as implemented in multielectron simulations, we refer the reader to the appendix of Ref. 52. To improve energy conservation in the nonequilibrium simulations, we reduced the time step to 0.5 fs.

B. Electron-molecule interactions

Interactions between the quantum electrons and the classical water molecules and sodium cation were represented by pairwise-additive one-body pseudopotentials. To keep our 2EM simulation details as close as possible to the previous 1EM (Ref. 46) and dielectron[52] simulations, we used the same electron-water pseudopotential, which was developed by Schnitker and Rossky.[48] This particular pseudopotential is based on the Philips–Kleinman (PK) theory, which imposes orthogonality constraints between the explicitly treated electron(s) and those treated implicitly through an added repulsive potential energy operator.[50,51] Thus, for consistency, we constructed an electron-sodium cation pseudopotential that is also based on the PK formalism. We had previously calcu-

lated the PK electron-sodium cation pseudopotential,[64] but the presence of sharp features in the core region (which is common with the PK method) made this potential unsuitable for use in molecular simulations. To overcome this issue, we used a method described in Appendix A to produce a pseudopotential that was both smooth in the core region and constrained to match the exact PK pseudopotential outside of the core region. This smoothed potential produces a neutral sodium atom valence electron wave function that matches the exact frozen-core Hartree–Fock (FCHF) valence wave function [i.e., the Na⁺ HF lowest unoccupied molecular orbital (LUMO)] outside the sodium core and has the same energy as the FCHF eigenvalue (i.e., the Na⁺ HF LUMO eigenvalue), -0.1818 hartree.[65] To approximately account for correlation effects between the explicitly treated valence electrons and the implicitly treated sodium cation core electrons, we added a polarization term to the sodium pseudopotential,

$$\hat{V}_{\mathrm{pzn}} = -\frac{\alpha}{2r^4} C(r), \tag{2}$$

where α is taken to be the experimental polarizability of a sodium cation in atomic units ($0.9457 a_0^3$), r is the electron-to-cation distance, and $C(r)$ is a damping function that prevents the polarization term from unphysically diverging near the nucleus of the sodium cation,

$$C(r) = 1 - \exp(-(r/\rho_{\mathrm{cut}})^6), \tag{3}$$

where we chose the cutoff parameter ρ_{cut} to be $1.5941 a_0$ in order to reproduce the experimental electron affinity of Na⁺. To test this potential, we calculated the gas-phase neutral sodium $3s$-$3p$ energy gap, which is responsible for the Na D-lines, to be 2.14 eV, which is in good agreement with the experimental values of 2.1023 and 2.1044 eV (we note that spin-orbit coupling is neglected in our calculations).[66] As a further test of our choice of parameters, we calculated the gas-phase electron affinity of sodium (i.e., the difference between the Na⁻ and Na⁰ ground-state energies) using the CISD method described in Sec. II C to be -0.49 eV, which is in reasonable agreement with the experimental value of -0.548 eV.[67] Having defined all interaction potentials, we are now in a position to discuss the method of solving for the electronic structure of our system.

C. Electronic structure method: CISD

To solve the electronic structure problem for the two valence electrons of sodide we used the real-space CISD method developed by Larsen and Schwartz.[52] In our 2EM, the quantum Hamiltonian for the two valence electrons of sodide is

$$\hat{H} = \hat{H}_1 + \hat{H}_2 + \hat{V}_{12}, \tag{4}$$

where $\hat{H}_i$ is the Hamiltonian for electron i (the kinetic energy operator and the external potential due to the classical particles) and $\hat{V}_{12} = e^2/|\boldsymbol{r}_1 - \boldsymbol{r}_2|$ is the Coulomb interaction between the electrons. The CISD method diagonalizes $\hat{H}$ in a basis of spin-adapted products of single-electron states. We

TABLE I. The convergence of CI eigenvalues, in eV, with the number of single-electron states N_{st} for a representative 2EM aqueous Na$^-$ solvent configuration.

N_{st}	E_0	E_1	E_2	E_3
8	−13.73	−10.84	−10.62	−10.40
12	−13.91	−11.34	−10.92	−10.61
16	−13.92	−11.35	−10.98	−10.76
20	−13.92	−11.36	−11.01	−10.78
24	−13.92	−11.37	−11.03	−10.78

consider only the spin-singlet manifold since we do not expect triplet states to play any significant role in CTTS dynamics. Following Larsen and Schwartz,[52] the particular single-electron states that we use to form the product basis are the single-electron adiabatic eigenstates; i.e., the eigenstates of $\hat{H}_1$.[68] We calculated these single-electron basis states by solving for the lowest N_{st} eigenvectors of $\hat{H}_1$ using an iterative and block-Lanczos diagonalization algorithm.[49] These one-electron eigenstates are expressed on a $16 \times 16 \times 16$ regular real-space cubic grid, so that the total number of grid points $N_g = 4096$. This grid-based representation allows for efficient application of the kinetic energy operator by Fourier transforming the wave functions to reciprocal space.[49] We set up the quantum grid at the center of the cubic simulation cell and chose the length of the quantum grid to be half that of the simulation box. This choice allowed us to use far fewer grid points than would be required to fill the whole simulation box and is justified because the spatial extent of the electrons' wave function was never more than a few angstroms, much smaller than either the 18.17 Å length of the quantum grid or the 36.34 Å length of the simulation cell. One consequence of using a quantum grid that is noncommensurate with the simulation cell is that periodic boundary conditions cannot be used in the quantum box. To avoid any errors inherent in the lack of periodicity, we made the quantum box large enough to prevent artifacts from arising due to the use of Fourier transforms, which assume periodicity, in evaluating the kinetic energy operator; this is why we did not choose a quantum grid that was smaller than half our simulation cell. In addition, we kept the wave function centered near the middle of the quantum grid to prevent "leakage" off the edge of the grid. This was accomplished by shifting the positions of all of the classical particles every 200 fs to force the electron's center of mass (as evaluated from the previous time step) to be near the center of the quantum box. We found that shifting the classical particles by an integral multiple of the quantum grid spacing prevented any discontinuity in the quantum energy.

To decide on the number of single-electron states to use to form our two-electron basis, we calculated the convergence of the CI eigenvalues with N_{st}; the results from a representative configuration for the ground (E_0) and first three excited states (E_{1-3}) are shown in Table I. We considered the calculation converged when any of the eigenvalues of interest did not change by more than 0.02 eV upon increasing the basis size. Based on this criterion, for the equilibrium ground-state simulations of aqueous sodide described in Sec.

III, we chose $N_{st} = 12$. For the nonequilibrium simulations in which sodide was excited to its lowest CTTS state that are described in Sec. IV, we chose $N_{st} = 16$. For the absorption spectrum and electronic structure of aqueous sodide that are described in Sec. III A 2, we chose $N_{st} = 20$. In their studies of the aqueous dielectron, Larsen and Schwartz[52] found a smaller basis of $N_{st} = 10$ to be adequate.

We were able to make use of larger bases after greatly improving the efficiency of the real-space CISD method. The slow step in the CISD method is the calculation of the matrix elements of the electron-electron Coulomb operator, which Larsen and Schwartz[52] evaluated with a piecewise constant approximation,

$$I_{abcd} = \frac{e^2}{a} \sum_{i=1}^{N_g} \sum_{j=1}^{N_g} \psi_a^*(\mathbf{r}_i)\psi_b(\mathbf{r}_i)\psi_c^*(\mathbf{r}_j)\psi_d(\mathbf{r}_j)\phi_{ij}, \quad (5)$$

where I_{abcd} is a matrix element between single-electron product states and $\psi_a\psi_c$ and $\psi_b\psi_d$,

$$\phi_{ij} = \int_{\text{cube } i} d\mathbf{r}_i \int_{\text{cube } j} d\mathbf{r}_j \frac{1}{r_{ij}} \quad (6)$$

is the electrostatic potential energy between two uniformly charged cubes, one centered at grid point i and the other centered at grid point j, and a is the spacing between quantum grid points. As written, the cost of forming these matrix elements scales as $N_g^2 N_{st}^4$. However, Eq. (5) can be rewritten as

$$I_{abcd} = \frac{e^2}{a} \sum_{i=1}^{N_g} \psi_a^*(\mathbf{r}_i)\psi_b(\mathbf{r}_i)W_{cd}(\mathbf{r}_i), \quad (7)$$

where

$$W_{cd}(\mathbf{r}_i) = \sum_{j=1}^{N_g} \psi_c^*(\mathbf{r}_j)\psi_d(\mathbf{r}_j)\phi_{ij} \quad (8)$$

is the Coulomb potential due to the charge density $\psi_c^*(\mathbf{r}_j)\psi_d(\mathbf{r}_j)$. Evaluating Eq. (8) for all product states is now the slow step, which scales as $N_g^2 N_{st}^2$. Thus, the leading scaling in our calculation has been reduced by a factor of N_{st}^2, which for $N_{st} = 12-20$ results in better than a hundred-fold speed up.

III. THE ROLES OF EXCHANGE AND CORRELATION IN THE EQUILIBRIUM PROPERTIES OF AQUEOUS SODIDE

In this section, we explore the equilibrium properties of aqueous sodide computed with our 2EM, and compare what we find in detail to the previous simulations that treated only one of the two sodide valence electrons quantum mechanically.[46] We also compare and contrast the behavior of our 2EM sodide in water with previous studies of the hydrated dielectron that used an identical simulation model but without the presence of the Na$^+$ core.[52–56] We begin by examining the ground-state electronic structure of this hydrated anion and then explore the relationship between the electronic structure and how this ion is solvated by liquid water. We close this section by investigating the unusual po-

TABLE II. Average properties of ground-state 1EM and 2EM aqueous sodide and the aqueous dielectron.

	Na_{aq}^- (2EM)[a]	Na_{aq}^- [b] (1EM)	$(e^-)_{2,aq}$ [c]
E_0 (eV)	−13.98(0.04)	−6.41 (0.04)	−5.99 (0.17)
E_I (eV)[d]	5.64(0.02)	7.91 (0.04)	1.60 (0.08)[e]
E_C (eV)	2.562(0.004)	⋯	2.57 (0.03)
E_{ex} (eV)	2.157(0.006)	⋯	2.08 (0.03)
R_{gyr} (Å) [f]	2.352(0.004)	1.546(0.004)	2.42 (0.03)
η [g]	0.056(0.001)	0.0225(0.0001)	0.14 (0.01)

[a]Properties of aqueous sodide in the 2EM averaged over our 200 ps ground-state simulation. The numbers in parentheses represent two standard deviations of the mean, calculated as described in Ref. 91.
[b]Properties of aqueous sodide in the 1EM averaged over a 72 ps simulation previously published (Ref. 46). The Coulomb and exchange energies, which are two-electron properties, do not exist in this model.
[c]Properties of the aqueous dielectron are taken from Ref. 53.
[d]Vertical ionization energy, defined by Eq. (10).
[e]Calculated from 10 ps of the simulation in Ref. 53.
[f]Radius of gyration of the valence electron density [Eq. (4) of Ref. 53].
[g]Symmetry order parameter [Eq. (9)].

larizability of the Na anion and provide a simple interpretation as to why this polarizability can only be properly described if both valence electrons are treated quantum mechanically.

A. The ground-state electronic properties of sodide in water

1. The size, shape, and energetics of ground-state aqueous sodide

For 1EM and 2EM aqueous sodide and the 2EM of the aqueous dielectron, Table II lists the ensemble-averaged values of the following equilibrium properties: The ground-state energy eigenvalue E_0; the vertical ionization energy E_I; the Coulomb and exchange energies (as defined by Eqs. (8)–(10) of Ref. 52), E_C and E_{ex}; the radius of gyration R_{gyr} of the ground-state wave function, which is a measure of the size of each species [see Eq. (4) of Ref. 53]; and the shape parameter η, which is defined as

$$\eta = \frac{2I_1 - (I_2 + I_3)}{2I_1 + I_2 + I_3}, \qquad (9)$$

where I_1, I_2, and I_3 are the principal moments of inertia of the charge density. For a perfect sphere, $\eta = 0$ and for an infinitely long rod, $\eta = 1$. We define the condensed-phase vertical ionization energy of each species by

$$E_I = -E(A^n) + E(A^{n+1}) + \epsilon, \qquad (10)$$

where $E(A^n)$ is the energy of the equilibrated species in oxidation state n, $E(A^{n+1})$ is the energy of the ionized species when the solvent is configured for the ground-state ion (i.e., without solvent rearrangement), and ϵ is the energetic cost of placing the ionized electron into the bottom of the liquid water conduction band. We can approximate $\epsilon \sim 1.5$ eV as the mean lowest adiabatic energy of an excess electron injected into neat water that is unequilibrated for the electron, which has been calculated in previous simulations that used the same electron-water pseudopotential as we use here.[49] Although this is a somewhat crude estimate of the conduc-

tion band onset, we note that the value we estimate does not affect any comparisons between the three solutes since ϵ is just a net additive constant to E_I. Since we truncate all interactions beyond a cutoff distance (see Sec. II), the ionization energies we report here will be lower bounds due to the neglect of the long-ranged solvent polarization around the negatively charged species beyond the cutoff radius. We note, however, that the truncation error in the ionization energies of the 1EM and 2EM sodide should be about the same, so that comparisons of their relative values are meaningful even if their absolute values are underestimates.

An examination of Table II shows that the electronic ground-state energy eigenvalue of 2EM sodide is much lower than the 1EM value: −14.0 and −6.41 eV, respectively. Of course, it is not meaningful to compare these values directly since, all else being equal, the 2EM system should have roughly twice the total energy of the 1EM system. Instead, it makes more sense to compare the vertical ionization energies E_I. The large E_I difference between the 2EM and 1EM sodide systems, 5.64 and 7.91 eV, respectively, is interesting because both models give similar gasphase ionization energies for sodide: In the 1EM, the sodium-electron pseudopotential was parameterized to exactly reproduce the experimental gas-phase ionization energy of $E_I = 0.547\,926$ eV,[67] and the 2EM gives $E_I = 0.49$ eV, as described in Sec. II B. Thus, the large difference between 2EM and 1EM aqueous sodide's E_I must be due to differences in the interaction of the ion with the solvent. Indeed, the values of R_{gyr} and η tell us that 2EM aqueous sodide is substantially larger and less spherical than in the 1EM, suggesting that the two model ions have very different interactions with the solvent, a point we shall explore in more detail in Sec. III B.

Although the 1EM and the 2EM of sodide have very different ground-state properties, Table II also reveals that 2EM aqueous sodide is remarkably similar to the aqueous dielectron. For example, aqueous 2EM sodide, despite having a cationic core that attracts the two electrons, has a radius of gyration that is only 0.07 Å smaller than the hydrated dielectron. Consequently, the electron-electron interactions in both ions are similar, as seen in the similar values of the Coulomb and exchange energies. We initially found it surprising that the presence of the attractive Na$^+$ core dramatically lowers the ground-state energy eigenvalue of 2EM sodide relative to the dielectron (the expectation value of the cation-electron potential is -13.20 ± 0.02 eV) but hardly modifies the electron density. However when we examined the electron-water interaction energy, we found that the expectation value of the water-electron potential energy operator is -9.48 ± 0.05 eV for 2EM aqueous sodide and ~ -14 eV (Ref. 69) for the hydrated dielectron. Thus, the lack of an attractive core in the dielectron is mitigated by the net additional negative charge that serves to attract the polar water solvent and compress the dielectron to a similar radius: In other words, the electrostriction of the first solvent shell surrounding the doubly charged dielectron compresses the two electrons' wave function to about the same extent as the presence of a singly charged cationic core.

Even though the size and electron-electron repulsion of

TABLE III. Spherical harmonic projections of the 2EM equilibrium sodide wave functions. (Calculated using the method described in Appendix B and averaged over 2000 solvent configurations from a 200 ps trajectory.)

State	E (eV)[a]	P_{ss}	P_{sp}	P_{sd}	P_{pp}
1	−14.0	79	9.5	1.3	6.4
2	−11.4	2.1	67	8.0	9.3
3	−11.2	2.2	63	9.4	9.5
4	−10.9	2.7	52	15	12
5	−10.6	1.8	11	38	32
6	−10.4	1.5	9.4	36	36
7	−10.2	2.2	6.9	37	36
8	−9.95	4.7	6.8	34	35
9	−9.76	6.3	6.9	30	37
10	−9.45	25	9.8	17	18

[a]Mean electronic energy eigenvalue.

2EM sodide and the dielectron are similar, there are some significant differences in the electronic properties of these systems. For instance, the dielectron has much lower vertical ionization energy than sodide, as expected for a doubly charged anion relative to a singly charged one. In addition, the hydrated dielectron has a relatively large asphericity, which has been discussed in detail in Ref. 53 and was explained as a Jahn–Teller-type symmetry breaking that serves to reduce electron-electron repulsion. The fact that 2EM aqueous sodide is much more spherical [2EM sodide has η =0.06, a value similar to that of the (single) hydrated electron] than the hydrated dielectron suggests that the cationic nucleus prevents such a Jahn–Teller-type distortion from taking place in aqueous sodide.

2. The electronic structure of equilibrium aqueous sodide

As discussed in Sec. I, the use of pseudopotentials to implicitly describe electrons that reside in the same shell as the explicitly considered electrons has been shown to lead to significant errors in the electronic structure of aqueous iodide.[47] Thus, in this subsection, we evaluate the importance of treating multiple valence electrons explicitly for CTTS calculations by examining the electronic structure of both 1EM and 2EM aqueous sodide. In the 1EM, aqueous sodide was found to have an s-like ground state with an average energy of −6.5 eV.[46] The solvent cavity supported three bound quasidegenerate p-like excited states, whose energies were split by the local asymmetry of the solvent cavity, at −2.0, −1.7, and −1.4 eV. Finally, the 1EM also had a series of unbound continuum states above 0 eV, which were characterized by considerable charge density spread throughout the entire simulation cell.[46]

For the 2EM, we analyzed the electronic structure of aqueous sodide by projecting the lowest ten adiabatic two-electron states onto spherical harmonic product states (see Appendix B). This analysis yields the angular correlation of the two-electron ground and excited states; we averaged the results, which are shown in Table III, over configurations drawn every 100 fs from the ground-state equilibrium trajectory. We see that the ground-state wave function has 79% ss character. We also see that the three lowest excited states of

aqueous sodide, at −11.4, −11.2, and −10.9 eV, have between 52% and 67% sp character. The angular nature of these states is consistent with what was seen in the 1EM. However, in contrast to the 1EM, we see that 2EM aqueous sodide has many additional bound excited states: Above the three mostly sp-character CTTS states is a whole manifold of bound excited states with a high percentage of sd and pp character; excitation to these states is thus very many-electron in nature.[70] Our examination of the charge densities of these excited states indicates that even though they are more diffuse than the ground state, they still lie mostly within the solvent cavity around the sodide ion: They are definitely not the continuum states seen in the 1EM. Indeed, the energies of these states are below the vertical ionization energy of sodide, consistent with these being solvent-supported bound CTTS states. Thus, we see that the 1EM of sodide captures the basic features of the three lowest CTTS states correctly, but misses the existence of many higher-lying CTTS states.

Even though the 1EM captures some of the basic features of the three lowest CTTS states, it fails to properly describe the detailed electronic character of these states. The energy gap between the ground and first excited states is substantially smaller in the 2EM simulation than the 1EM simulation (2.6 and 4.5 eV, respectively), which is a direct consequence of treating the electron-electron interaction explicitly. In addition, Table III shows that 2EM aqueous sodide has non-negligible double-excited character in its ground and first three excited states. For example, the ground state of 2EM sodide in water has an average of 6.4% pp character, which is due entirely to configuration mixing resulting from electron correlation.[71] This behavior could never be captured in a 1EM because the use of the pseudopotential assumes that the implicitly treated electron remains in an atomic $3s$ state regardless of the state of the other electron. Thus, it is critical to have an appropriate treatment of exchange and correlation to correctly determine the electronic structure of CTTS anions.

3. The optical absorption spectrum of aqueous sodide

The differences in the calculated electronic structure of the 1EM and 2EM aqueous sodides are manifested most clearly in the calculated optical absorption spectrum. We calculated the absorption spectrum of aqueous sodide in the inhomogeneous limit using the formalism outlined in Eq. (10) of Ref. 53; the results are shown as the solid curves in Figs. 1(a) and 1(b) for the 1EM and 2EM, respectively. The dashed curves in these figures show the densities of energy gaps between the ground state and the excited states that comprise the absorption bands. Figure 1(a) shows that for the 1EM, the sodide CTTS band results entirely from transitions between the s-like ground-state and the three quasidegenerate p-like CTTS excited states, peaking at 4.65 eV. These three transitions are strongly dipole allowed, and the higher-lying continuum states contribute virtually nothing to the absorption spectrum. Figure 1(b) shows that the CTTS band of 2EM aqueous sodide, like that of 1EM sodide, arises mostly from transitions to the three lowest sp-like CTTS excited
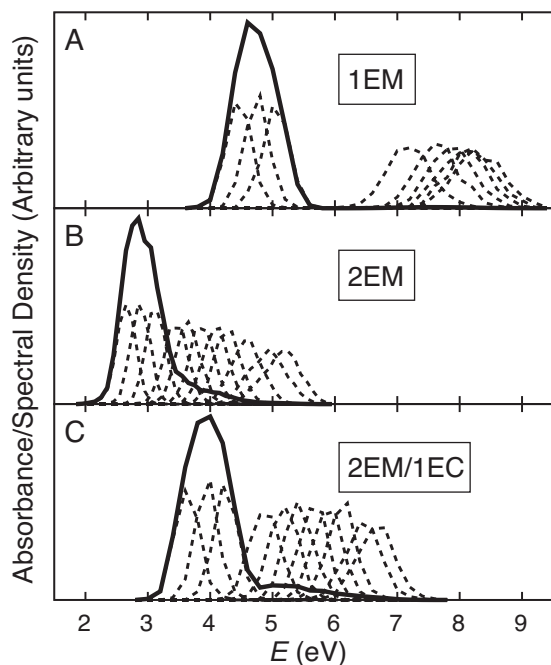
FIG. 1. The optical absorption spectrum of aqueous sodide (solid curves) as calculated in the 1EM [panel (a)], equilibrated 2EM [panel (b)] and 2EM with one-electron-model solvent configurations [2EM/1EC, panel (c)]. Also shown are distributions of energy gaps between the ground and first eleven excited states (dashed curves).

states, which are strongly dipole allowed from the ss-like ground state. The 1EM and 2EM spectra, however, show two significant differences. First, the 2EM spectrum has a blue tail that is not present in the 1EM spectrum. Second, all of the transitions occur at a much lower energy in the 2EM than in the 1EM: The absorption maximum for 2EM aqueous sodide is at 2.80 eV, almost 2 eV redder than that in the 1EM. We explore each of these differences in turn.

The blue tail seen in the 2EM aqueous sodide CTTS absorption spectrum is relatively easy to assign: This blue tail is the result of transitions from the ground state to the bound excited states of mixed pp and sd character that lie higher in energy than the three principle sp-like CTTS states. Higher-lying states are completely absent in the 1EM, and transitions to these states are weakly allowed in the 2EM because of the small amount of sp-character in the ground state (Table III). The presence of this blue absorption tail is in good accord with experiment since the absorption spectrum of sodide in moderately polar solvents such as ethers and amines looks very much like the 2EM spectrum shown here.[72,73] We can also compare the absorption spectrum of 2EM aqueous sodide to that of the hydrated dielectron. Larsen and Schwartz[53] found that the absorption spectrum of the hydrated dielectron peaked at around 3 eV and was predominantly due to transitions from an ss-like ground state to three sp-like excited states. The dielectron absorption spectrum also had a blue tail due to the presence of many bound solvent-supported excited states. Thus, the electronic structure of aqueous sodide appears remarkably similar to that of the solvated dielectron; the main effect of the sodium cation core is to lower the absolute energies of the bound states.

Another significant difference between the 1EM and

2EM calculated aqueous sodide spectra, seen in Fig. 1, is the large redshift of the 2EM CTTS spectrum relative to the 1EM CTTS spectrum. Although we know that this large redshift of the CTTS band results from the improved treatment of exchange and correlation in the 2EM, how much of the shift simply arises from the use of a higher level of theory for the electronic structure and how much comes from changes in the local solvent environment that result from the different sizes and shapes of the sodide ion between the two models? To answer this question, we calculated the absorption spectrum of sodide taking solvent configurations from the 1EM trajectory but using the CISD electronic structure method of the 2EM; we will refer to this calculation as 2EM/1EC (2EM with one-electron configurations). This calculation is reminiscent of the previous calculations of Bradforth and Jungwirth,[47] who explored the nature of aqueous iodide's CTTS electronic structure using a simulation where the solvent was not equilibrated with the quantum solute but rather with a similar ion (in their case, a classical iodide ion). Since we have the full equilibrium dynamics of the 2EM for aqueous sodide, we can use our 2EM/1EC calculations to test the accuracy of QM/MM-like simulations that perform high-level electronic structure calculations with molecular geometries found using a lower level of theory. For our 2EM/1EC calculation, we diagonalized the CISD Hamiltonian using the potentials described above in Sec. II B for 500 snapshots, drawn every 200 fs, from the 1EM trajectory of 200 water molecules and a sodium anion.[46] The aqueous sodide density of energy gaps and absorption spectrum that we calculate for the 2EM/1EC are plotted in Fig. 1(c). The 2EM/1EC model gives a nearly identical overall electronic structure as the full 2EM, but the CTTS band lies between the 1EM and 2EM spectra, with a calculated absorption maximum at 3.95 eV. Thus, we see that the improved quantum treatment of sodide's valence electrons in the 2EM is only partly responsible for the redshift of the 2EM spectrum relative to the 1EM spectrum: A significant fraction of the redshift in the 2EM must result from a change in the solvent structure that accompanies the more accurate electronic treatment. We will explore the details of this change in solvent structure in the next section. Overall, our exploration of the 2EM/1EC shows that hybrid models using high-level electronic structure on configurations generated from a lower level of theory can provide correct qualitative pictures of electronic structure but at the expense of quantitative accuracy.

B. The equilibrium solvent structure of aqueous sodide

The large redshift of the aqueous sodide CTTS absorption spectrum in the 2EM relative to the 2EM/1EC seen in Fig. 1 indicates that there must be a significant difference in the solvent structure of aqueous sodide in the 2EM and the 1EM. In this section, we analyze the solvent structure from the 1EM and 2EM simulations in detail in order to understand how use of the 2EM leads to a qualitatively different solvent structure around the anion.

Figure 2 compares radial pair distribution functions, $g(r)$, for sodium nucleus/water-site separations calculated
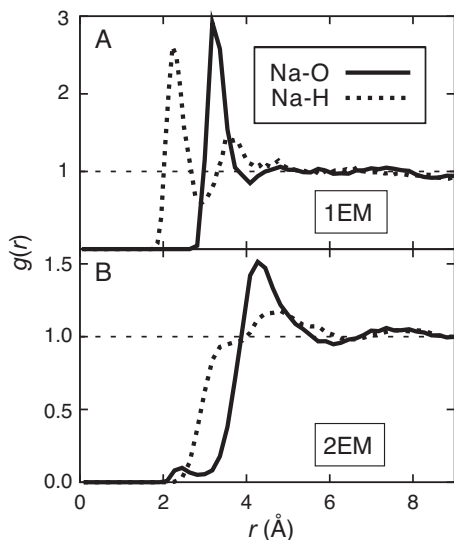
FIG. 2. Radial distribution functions (RDFs) for water site-sodium displacements of ground-state aqueous sodide calculated both in the 1EM [panel (a)] and 2EM [panel (b)]. Oxygen-sodium RDFs are plotted as solid curves; hydrogen sodium RDFs are plotted as dashed curves.

from both the 1EM [panel (a)] and the 2EM [panel (b)]. The solvent structure seen in the 1EM is fairly typical for an aqueous anion. There is a clear peak in $g_{Na-O}(r)$ at 3.2 Å that indicates the position of the first solvation shell, and a corresponding peak in $g_{Na-H}(r)$ that is 1 Å closer to the sodium nucleus. Since the O–H bond length of our model of water is 1.0 Å, this indicates that the 1EM sodium anion is H-bond solvated by the first-shell water molecules. In contrast, the solvent structure associated with the 2EM is quite different. The peak in $g_{Na-O}(r)$ occurs out at 4.2 Å, is much broader and has a smaller maximum value than that in the 1EM. In addition, there is no well-defined peak in the 2EM $g_{Na-H}(r)$; instead, there is only a shoulder near 3.2 Å that indicates that the 2EM anion is only partially H-bond solvated.

We can integrate the pair distribution functions in Fig. 2 from the origin to the first minimum to determine the average number of each type of solvent site in the first solvation shell of the two model anions. For the 1EM, if we choose the first solvent shell to lie within 2.9 Å for water H sites and 4.0 Å for water O sites, we obtain coordination numbers of 7.0 and 9.5 for the H and O sites, respectively. In contrast, if we choose the first solvent shell to lie within 3.7 Å (the edge of the shoulder) and 6.0 Å for the H and O sites in the 2EM, we find coordination numbers of 7.4 and 25 for H and O sites, respectively. Thus, most (on average, 7 out of 9.5) of the first-shell waters in the 1EM form an H bond to the sodium anion. In contrast, despite a very large first solvation shell (25 waters) in the 2EM, there are still only about 7 H bonds to the sodium anion. Clearly, the inclusion of exchange and correlation makes the solvent structure around aqueous sodide quite different for the 2EM relative to the 1EM.

How does the explicit inclusion of correlation account for these structural differences? We believe that most of these structural differences arise from the large difference in ion size between the 1EM and the 2EM (cf. Table II, above). We can invoke a simple scaling argument to equate the num-

ber of first solvation shell waters to the 1EM and 2EM anion surface areas: Using the electronic radii of gyration as a measure of the anion size, simple scaling predicts that 2EM sodide should have $\sim (2.352/1.546)^2 = 2.3$ times as many first-shell waters as 1EM sodide, which is close to what we see. The observation that water forms about as many H-bonds to 1EM sodide as 2EM sodide despite the larger solvation shell of the latter is presumably a result of there being an energetic penalty associated with breaking more than seven water-water H bonds to form an additional H bond to sodide. This limiting H-bond behavior also has been observed in recent *ab initio* MD computer simulations of the aqueous halides,[74–76] which showed that water forms only approximately five H bonds to fluoride, chloride, and iodide despite the fact that the number of first-shell water molecules increases from 5.0 to 5.8 to 6.6, respectively. In other words, the difference in solvation structure of 2EM and 1EM sodide is attributable to the larger size of the 2EM anion and the fact that liquid water solvates smaller anions better than larger anions.

It is interesting to note that the 1EM anion has a radius of gyration of 2.8 Å in the gas phase, which is larger than the gas-phase 2EM anion's value of 2.299 Å. Thus, the 1EM anion is considerably compressed when dissolved in water, but the 2EM anion is not. This can be explained by considering the differences in the 1EM and 2EM Hamiltonians. In the 1EM, only the kinetic energy term disfavors compressing the electron since the electron-sodium core interaction is attractive. In the 2EM, however, the electron-electron exchange and Coulomb energies also disfavor compressing the sodide ion. The 1EM's radial pair distribution functions in Fig. 2 reveal precisely what is happening: In the 1EM, the Na–O pair distribution function turns on very rapidly at ~ 2.8 Å and peaks at around 3.2 Å, a distance that matches the Lennard-Jones Na–O diameter.[46] Thus, it is the classical Na–O interaction that dictates how close the solvent can approach the 1EM anion, not the quantum electron-solvent interaction. This is obviously problematic since the 1EM classical Na-solvent interaction is parametrized for a neutral species, not an anion. This idea that the classical Na–O interaction is what controls the solvent structure also explains why 1EM sodide is more spherical than 2EM sodide.

Despite the much larger size of the 2EM aqueous sodide anion compared to the 1EM anion, Fig. 2(b) shows that there is a small peak in the 2EM $g_{Na-O}(r)$ at 2.3 Å that is absent for the 1EM; this peak indicates that oxygen atoms on nearby water molecules occasionally are able to get much closer to the 2EM sodium nucleus than they can get to the 1EM nucleus. If we integrate this peak from the origin to the minimum at 2.9 Å, we obtain a value of 0.14, suggesting that roughly 14% of the time, a water O atom resides within 2.9 Å of the 2EM sodium nucleus. This peak is in the same position as the first solvation shell peak of the $g_{Na-O}(r)$ for a dilute Na^+ aqueous solution,[77] which indicates that sometimes, water is actually directly solvating the cationic core of the 2EM sodium anion. To explore this in more detail, we calculated a coordination number of the 2EM sodium cation core n_{Na^+} by counting the number of configurations that have oxygen atoms within 2.9 Å of the sodium cation. We found

that of 10 000 configurations that we examined, the sodium cation core is coordinated by one O atom $\sim$13% of the time, two O atoms $<$1% of the time, and is uncoordinated for the remaining $\sim$86% of the time. In fact, this core-solvation structural motif has been seen previously in theoretical studies of gas-phase sodide-water clusters, $Na^-(H_2O)_n$, by Hashimoto et al.[78] These authors applied *ab initio* structural optimization to clusters with $n \leq 4$ and found local minima in which the oxygen atom of water was only $\sim$2.3 Å from the sodium, the same separation that we see in Fig. 2. Moreover, even though Hashimoto et al.[78] found that the lowest-energy structure for a given n was H-bond solvated, they also saw that the structures involving oxygen atom coordination were typically only 1–3 kcal/mol higher in energy, implying that these structures should be readily accessible at room temperature. This suggests that both in clusters and in the condensed phase, the solvent is capable of pushing the two valence electrons of Na^- far enough to completely expose the sodium core, thus gaining favorable water-cation interactions at the expense of distorting the electronic structure of the anion. We will examine the consequences of this unusual polarizability of the aqueous sodium anion in detail in Sec. III C.

To analyze the changes in the solvent structure that occur when the 2EM Na^+ core of sodide is partially solvated by the O atoms of water, we grouped configurations by their value of n_{Na^+}. We then calculated cylindrical pair distribution functions (CDFs), $g_{cyl}(z, \rho)$, to examine the solvent structure for each of the groups. In our CDFs, we defined the positive z-axis of the cylinder as the line from the sodium nucleus to the valence electrons' center of mass; thus, the z-axis also points along the instantaneous dipole moment of the anion, which will be discussed in more detail in Sec. III C. With this definition of the z-axis, the CDFs allow us to probe the solvent structure on both the core and electron sides of the distorted anion, providing information that cannot be obtained from a radial distribution function (RDF). We calculated the CDFs via

$$g_{cyl}(z, \rho) d\rho \, dz = \left\langle \frac{1}{2\pi\rho n} N(\mathbf{r}) d\mathbf{r} \right\rangle, \quad (11)$$

where the origin is the sodium nucleus, $N(\mathbf{r})d\mathbf{r}$ is the number of solvent sites within a small volume $d\mathbf{r} = \rho d\rho d\phi dz$ of the position $\mathbf{r}$, ρ is the distance perpendicular to the z axis, n is the number density of solvent sites, and the brackets denote an equilibrium ensemble average over the appropriate group. We averaged our CDFs using histogram bin widths of $\Delta z = \Delta \rho = 0.5$ Å. Contour plots with 0.2 spacing of the CDFs for groups 1 and 0 are shown in Figs. 3 and 4, respectively; there were too few uncorrelated configurations in group 2 to generate a statistically meaningful CDF. The contour levels above 2.0 in both figures have been omitted for clarity, and the position of the global maximum in the group 1 CDFs in Fig. 3 is indicated by a "$\times$" symbol.

Examination of Fig. 3 shows that both the O-site [panel (a)] and H-site [panel (b)] group 1 CDFs have a prominent peak on the cationic side of the distorted anion ($z<0$): The O-site CDF peaks at coordinate (-2.25 Å, 0.25 Å) with value of 9.95, and the H-site CDF peaks at coordinate
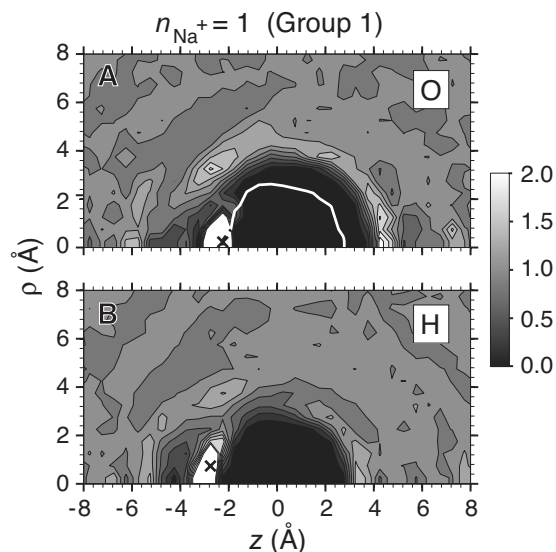
FIG. 3. CDFs [Eq. (11)] of water-sodium displacements for configurations in group 1, which have one water oxygen site within 2.9 Å of the 2EM aqueous sodide cationic core. The oxygen CDF is plotted in panel (a) and the hydrogen CDF is plotted in panel (b). The origin is the position of the sodium cation and the z-axis points in the direction of the electron center of mass. Contour levels are separated by 0.2. No contour levels are plotted above 2.0; instead, the positions of the peaks in the CDFs are represented by a $\times$ symbol. The hydrogen CDF 0.2 contour is shown as a white curve on the oxygen CDF [panel (a)].

(-2.75 Å, 0.75 Å) with value of 3.83. Since the peak in the O-site CDF is the only feature within 2.9 Å of the origin, this peak (and the corresponding peak that is $\sim$1 Å further away in the H-site CDF) must correspond to a single water molecule that is preferentially aligned so that the O atom is closest to the sodium cation core. On the electron side of the anion ($z>0$), the H-site CDF turns on closer to the origin than the O-site CDF, as can be seen most easily by comparing the lowest contour levels ($g_{cyl}=0.2$) of the H-site CDF [plotted as the white curve in panel (a)] and O-site CDF. Thus, Fig. 3 shows highly asymmetric solvation of the anion
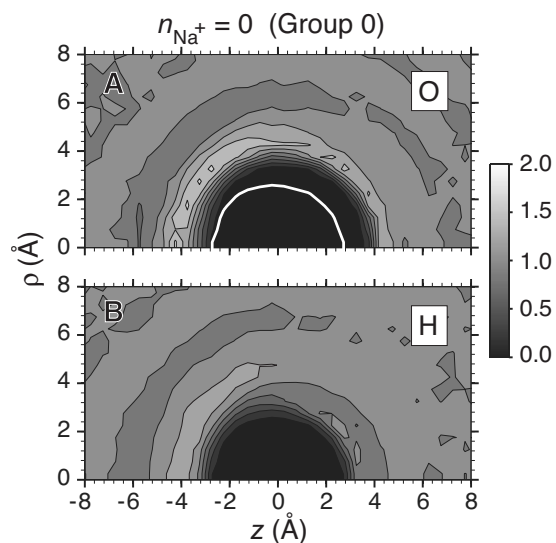
FIG. 4. CDFs of 2EM aqueous sodide, same as Fig. 3, but for configurations in group 0, which have no water oxygen sites within 2.9 Å of the sodium cationic core.

in the group 1 configurations: On the electron-deficient side of 2EM sodide, water is preferentially oriented so that its O atom is close to the sodium cation core, while on the electron-rich side, water is preferentially oriented so that its H atoms are close to the sodide valence electrons. A similar, although less pronounced, asymmetric solvation is seen in Fig. 4 for the group 0 CDFs. There are no prominent peaks in the group 0 CDFs because there are no water molecules in close proximity to the sodium cation core in these configurations. However, the local solvent environment is still asymmetric: The O-site CDF's 0.2 contour is shifted such that it is closer to the origin for $z<0$ than for $z>0$, and the reverse is true in the H-site CDF. This means that in most configurations, the local solvent environment exerts a net electric field on the 2EM sodium anion: The negatively charged oxygen sites of some water molecules tend to be closer to one side of the sodide anion while the positively charged hydrogen sites of some water molecules tend to be closer to the opposite side. The presence of this electric field has profound consequences for the electronic structure of the anion, which we explore in Sec. III C.

C. The polarizability of aqueous sodide

The fact that the solvation structure around the 2EM aqueous sodide ion is asymmetric implies that the anion itself, on average, is distorted from spherical symmetry. One measure of this distortion of the anion is the instantaneous dipole moment,

$$\boldsymbol{\mu}(t) = \langle \Psi(\boldsymbol{r}_1,\boldsymbol{r}_2;t) | (\hat{\boldsymbol{r}}_1 + \hat{\boldsymbol{r}}_2) | \Psi(\boldsymbol{r}_1,\boldsymbol{r}_2;t) \rangle = \int \rho^{(2)}(\boldsymbol{r};t)\boldsymbol{r}\, d\boldsymbol{r},$$

(12)

where we choose the origin of the coordinate system to be the position of the classical sodium cation core and $\rho^{(2)}$ is the two-electron charge density (normalized to 2).[79] Figure 5(a) shows the time evolution of the magnitude of $\boldsymbol{\mu}$ over a portion of the 2EM ground-state trajectory. The large deviations from zero tell us immediately that the solvent is indeed inducing a large dipole moment on the sodium anion, reaching values of over 3 e Å (14 D), which is a substantial dipole moment for an atomic anion! The solid curve in Fig. 5(b) shows the distribution of the magnitude of the dipole moment calculated from the full 200 ps 2EM equilibrium simulation. The most probable value of μ is $\sim$0.8 e Å, compared to a value of $\sim$0.1 e Å in the 1EM. Clearly, accounting for the exchange and correlation of the sodide valence electrons is critical to describing the large polarizability of the solvated anion. We also see that the magnitude of the dipole moment correlates well with the value of the shape parameter for the ground-state electron density, η [Eq. (9)]. It is thus the large polarizability of sodide that explains the asphericity of the average charge density.

We note that the effects of a solvent on the electronic structure of dissolved atoms have been explored in the previous theoretical work. For example, using a continuum dielectric liquid model, Logan[80] found that under certain conditions, reaction fields set up in the liquid can be sufficient to stabilize an induced dipole moment on a dissolved atom, a
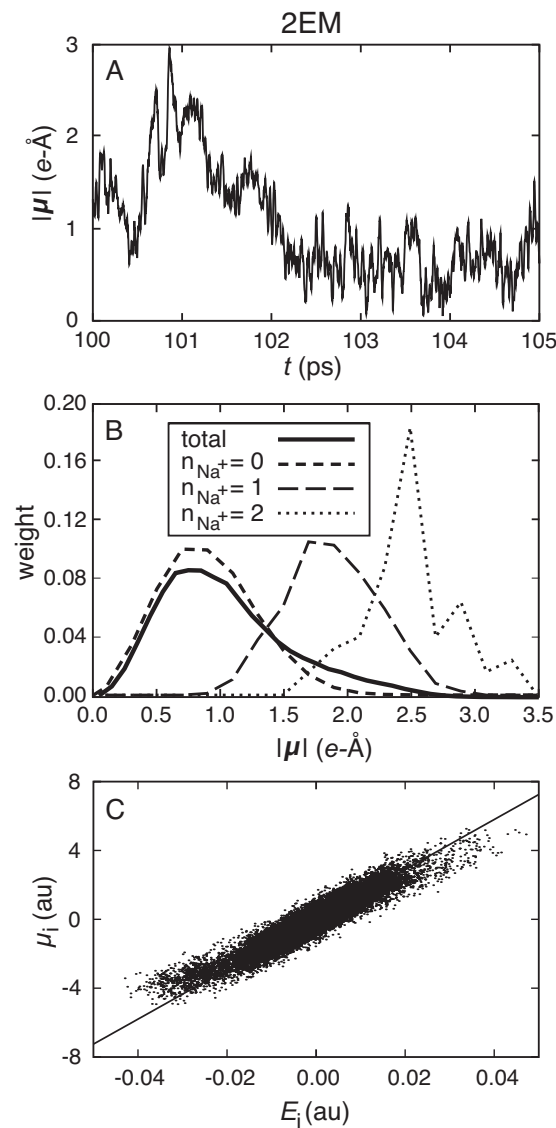
FIG. 5. Properties of the induced dipole moment, $\boldsymbol{\mu}$, on 2EM sodide. Panel a shows a representative 5 ps time trace of $|\boldsymbol{\mu}|$ taken from our equilibrium ground-state trajectory. Panel b shows area-normalized distributions of $|\boldsymbol{\mu}|$ calculated with a histogram bin width of 0.1 e Å: The solid curve is the distribution of $|\boldsymbol{\mu}|$ calculated from all configurations; the short dashed curve is the distribution calculated from configurations in group 0, where no water oxygen atoms are coordinating the sodium cation ($n_{Na^+}=0$); the long-dashed curve is the distribution for group 1 and the dotted curve is for group 2. Panel c is a scatter plot showing the correlation between the Cartesian components of the electric field at the sodium cation E_i and the same Cartesian component of μ_i, all in a.u. Also plotted is a best-line fit of $\mu_i=145E_i$.

so-called dipolar excitonic state. Simulations by Dobrosavljevic et al.[81] also found that an unpolarizable hard-sphere liquid was able to induce mixing of s and p states in an atomic solute. It is thus interesting to explore whether the large dipole moment on 2EM sodide is induced by solvent electric fields or by the solvent's short-range repulsive interactions. When we analyzed our simulations, we found no correlation between the repulsive sodide-solvent potential energy and the magnitude of the dipole moment, but we did find a striking correlation with the magnitude of the local electric field. We calculated the local electric field at the anion as a simple sum of Coulombic fields from the partial charges on the classical water molecules,

$$E(\mathbf{r}) = \sum_i \frac{q_i(\mathbf{r}_i - \mathbf{r})}{|\mathbf{r}_i - \mathbf{r}|^3}, \tag{13}$$

where the sum is over all atomic sites (O and H) in the simulation, q_i is the partial charge of atomic site i, and $\mathbf{r}_i$ is the position of atomic site i. Figure 5(c) shows the correlation between the vector components of the electric field and the induced dipole moment of the sodide anion (the x, y, and z components are overlaid); the correlation is strikingly linear, with a correlation coefficient of 0.94, firmly supporting the idea that the dipole moment is induced by the solvent's local electric field. The proportionality constant, which is the polarizability of the sodide solute, is found to be $\sim 145 a_0^3$. We note that at the highest electric fields, there is some deviation from linearity between induced dipole moment and electric field as the induced dipole tends to saturate, suggesting that 2EM sodide has a negative hyperpolarizability.

A polarizability of $145 a_0^3$ makes aqueous sodide an incredibly polarizable anion: For comparison, aqueous iodide's polarizability is only $49.97 a_0^3$.[82] To understand how this value arises from the electronic structure of 2EM sodide, we calculated the polarizability tensor of the sodium anion in our simulation directly using the standard sum-over-states formula,[83]

$$\alpha_{ij} = 2 \sum_{n>0} \frac{\langle \Psi_0 | er_i | \Psi_n \rangle \langle \Psi_n | er_j | \Psi_0 \rangle}{E_n - E_0}, \tag{14}$$

where i and j refer to Cartesian directions, $\langle \Psi_n | er_j | \Psi_0 \rangle$ is the jth Cartesian component of the transition dipole moment between electronic state 0 (the ground state) and electronic state n, and $E_n - E_0$ is the energy gap between these states. Although the sum in Eq. (14) is formally infinite, we evaluated the polarizability of aqueous Na^- by summing only over the 209 excited states obtained from our CISD calculation. This truncation is reasonable for two reasons. First, the energy gap in the denominator damps out contributions from highly excited states. Second, the transition dipole moments in the numerator are only large between the ground state and first few excited states, as we showed above in our calculation of the sodide absorption spectrum; in fact, we found that contributions from the lowest ten excited states made up most of the polarizability tensor. Using Eq. (14), we calculated the ensemble-averaged polarizability tensor elements in atomic units to be $\alpha_{xx} = 168 \pm 7$, $\alpha_{yy} = 171 \pm 7$, $\alpha_{zz} = 167 \pm 7$, $\alpha_{xy} = 2 \pm 5$, $\alpha_{xz} = -3 \pm 5$, and $\alpha_{yz} = -1 \pm 5$. Thus, the isotropic polarizability is $\alpha_{iso} = 169 \pm 4$ and the anisotropic elements average to zero within our statistics. This direct calculation of sodide's polarizability agrees rather well with our simple estimate based on the dipole-field correlation seen in Fig. 5(c).[84] The small discrepancy is likely due to contributions from the anisotropic components, which although they average out to zero, have instantaneous magnitudes of up to $\sim 50 a_0^3$.

If we use Eq. (14) with 253 CI-product basis states to calculate the polarizability of 2EM gas-phase sodide, we obtain a value of $1062 a_0^3$, which is in excellent agreement with a previous CCSD(T)-level calculation that found $\alpha = 1034 \pm 10 a_0^3$.[85] This means that sodide undergoes a dramatic reduction in polarizability when interacting with the water solvent. This reduced polarizability in the liquid is particularly interesting given that the size of the anion in solution is roughly the same as in the gas phase: The calculated radii of gyration of Na^- are 2.352 ± 0.004 and 2.299 Å in water (Table II) and in the gas phase, respectively. Thus, the reduction in polarizability upon aqueous solvation must be a result of solvent-induced changes in the electronic structure of sodide. Indeed, we see that $\sim 80\%$ of our calculated gas-phase polarizability comes from transitions to three virtual states with p-symmetry at ~ 1.5 eV above the ground state (~ 1 eV above detachment). In contrast, the lowest band of p-like excited states (the CTTS states) for sodide in solution is found near 2.8 eV. Thus, even though confinement by the solvent makes the virtual excited states become bound, the fact that the solvent raises the energy of these excited states is responsible for the reduced polarizability in aqueous solution compared to the gas phase.

Finally, we can examine the correlation between the induced dipole moment on 2EM aqueous sodide and the local solvent structure. The various dashed curves in Fig. 5(b) examine the distribution of induced dipole moments averaged for the same groups of configurations that we employed in the previous section (i.e., configuration groups in which 0, 1, or 2 water O atoms lie within 2.9 Å of the sodium cation core). Each of the three groups shows a broad distribution of induced dipole moments with a width of ~ 1 e Å, but the centers of the distributions move to larger $|\boldsymbol{\mu}|$ on going from group 0 (0.8 e Å) to group 1 (1.8 e Å) to group 2 (2.5 e Å). Thus we see a correlation between $|\boldsymbol{\mu}|$ and n_{Na^+}; configurations with $n_{Na^+} = 2$ or 1 tend to have a larger $|\boldsymbol{\mu}|$ than configurations with $n_{Na^+} = 0$. This suggests that when a large electric field is incident on the sodide anion, the sodide valence electrons are displaced and vice versa, leaving the cationic core to be solvated by the negatively charged O atom of water. Thus, even though there is an energy penalty to distort the electronic structure of the anion and mix in higher-lying configurations, it is still energetically favorable for water to distort the anion: Not only is there a favorable dipole-induced dipole interaction, but if the electrons are displaced far enough, the solvent can directly interact with the sodium cation core. Once the electrons are displaced enough to expose the core, however, there is no additional energetic advantage to distorting the anion further, explaining why the induced dipole saturates at high electric fields.

IV. NONADIABATIC RELAXATION OF EXCITED SODIDE

In Sec. III C, we found that the electronic and solvation structure of equilibrium aqueous sodide is qualitatively different in the more accurate two-electron simulations than in one-electron simulations. In this section, we consider the relaxation dynamics of aqueous 2EM sodide following excitation to the lowest CTTS state. Since our main interest is to build a qualitative picture of the differences between the 2EM and 1EM, we have not attempted to simulate an experimentally realistic response of 2EM sodide following CTTS excitation (i.e., averaging over many nonequilibrium trajec-
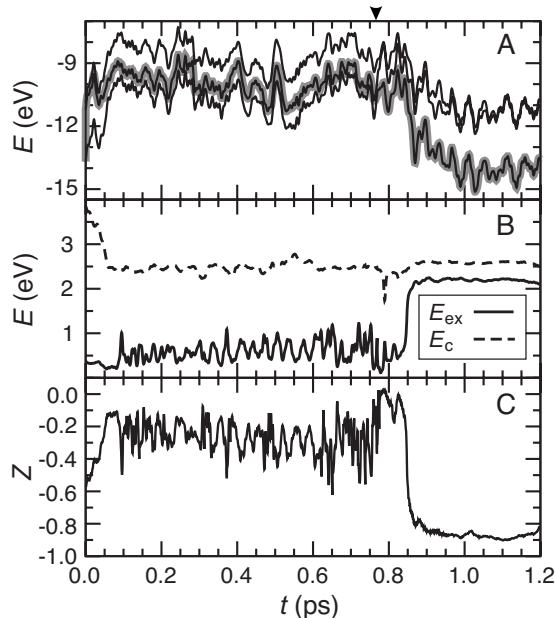
FIG. 6. Properties of one of the nonequilibrium trajectories of excited 2EM aqueous sodide that correspond to a detachment pathway. The time of nonadiabatic transition to the ground state is indicated by the arrow. The lowest three adiabatic energies are plotted in panel (a) as solid curves; the occupied mean-field state energy is plotted as the thick gray curve. Panel (b) shows the exchange and Coulomb energies, E_{ex} and E_C, respectively, for the occupied adiabatic state. Panel c shows the integrated charge from the mean-field state electron density within 3.6 Å of the sodium nucleus Z.

tories). Instead, to reduce the computational expense, we have explored a relatively small nonequilibrium ensemble of 13 trajectories, each started from configurations taken from the 2EM equilibrium aqueous sodide simulation that were separated by at least 1 ps and had the lowest CTTS state lying 2.45 ± 0.03 eV above the ground state. Of these 13 initial configurations, 6 are from group 0 (the group with no water oxygen solvating the sodium cation core), 4 are from group 1 (one water oxygen solvating the sodium cation core), and 3 are from group 2 (two water oxygens solvating the sodium cation core). In a statistical ensemble, only approximately two configurations would have been from group 1 and none would have been from group 2; we chose to consider this nonstatistical selection, however, to analyze the influence of the close-lying water molecules that occasionally solvate the Na$^+$ core on CTTS dynamics. Despite our use of the nonstatistical set of initial configurations, we found no correlation between the excited-state lifetime of sodide in our nonequilibrium trajectories and the presence or absence of water molecules solvating the sodium cation core. We did find, however, that the presence of water molecules close to the cation core made detachment of one of the excited electrons more likely, a result we discuss in more detail below in Sec. IV B.

A. The CTTS dynamics of 1EM and 2EM aqueous sodide

Figures 6–8 plot several dynamical properties from three of our 2EM nonequilibrium trajectories, including the mean-field (occupied) electronic energy and lowest adiabatic electronic energies [panel (a)], the exchange and Coulomb ener-
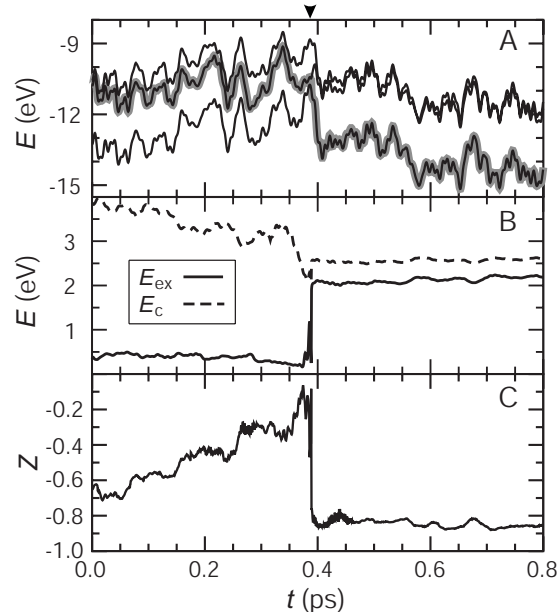
FIG. 7. Properties of one of the nonequilibrium trajectories of excited 2EM aqueous sodide as for Fig. 6 but for a trajectory corresponding to a nondetachment pathway.

gies of the occupied state [defined by Eqs. (8)–(10) of Ref. 52; panel (b)], and the net charge of the sodium species [defined as the sum of the cation core charge plus the integrated electron density within 3.6 Å of the sodium cation,[86] panel (c)]. We break our discussion of these 2EM nonequilibrium sodide trajectories into two parts, first examining the short-time excited-state dynamics and then focusing on longer-time behavior associated with nonadiabatic return to the ground state.
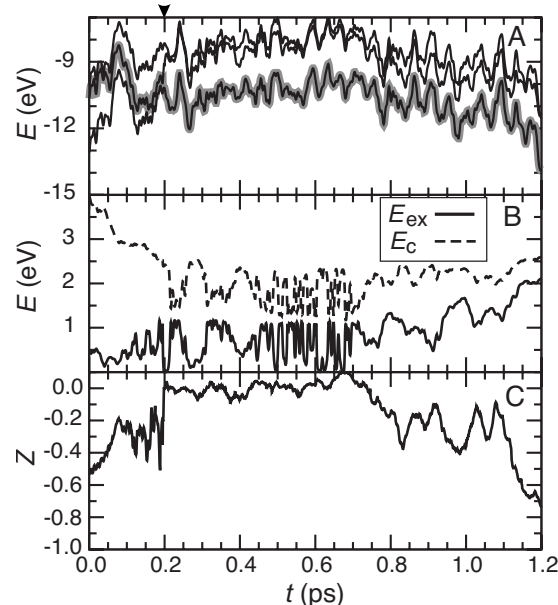
FIG. 8. Properties of one of the nonequilibrium trajectories of excited 2EM aqueous sodide as for Fig. 6 but for a trajectory corresponding to a detachment pathway in which the Na$^+$ core is solvated by two water oxygen atoms (i.e., the initial configuration was from group 2).
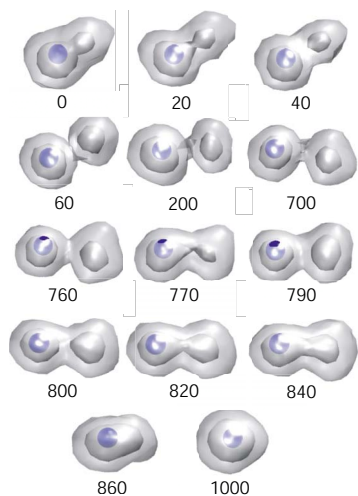
FIG. 9. (Color online) Time snapshots of the mean-field 2EM aqueous sodide electron density during the detachment pathway shown in Fig. 6. The sodium cation is represented as a blue sphere with the ionic radius of Na$^+$. The electron density is plotted as two surfaces: One at 0.016 (encompassing ~50% of the charge density) and another at 0.0025 (encompassing ~90% of the charge density). The numbers correspond to femtoseconds after excitation; the nonadiabatic transition to ground state occurs at 769 fs.

1. Short-time dynamics following CTTS excitation of 2EM aqueous sodide

In all 13 of our 2EM nonequilibrium trajectories, we found that the CTTS excited-state dynamics prior to the nonadiabatic transition to the ground state were virtually identical, as can be seen in the representative trajectories shown in Figs. 6–8. In panel (a) of each of these figures, the heavy gray line marks the energy of the occupied mean-field quantum state. In all of our trajectories, the mean-field state is nearly entirely comprised of the lowest adiabatic CTTS excited state; in fact, we never saw more than 10% mixing with the second adiabatic excited state in any of our nonequilibrium trajectories. Thus, the CTTS dynamics of 2EM aqueous sodide takes place essentially on a single adiabatic energy surface until the time when the system makes its nonadiabatic transition to the ground state. In all of our nonequilibrium trajectories, the solvent moves during the first few hundred femtoseconds following excitation to solvate the occupied lowest CTTS state. Since the solvent cavity becomes elongated to accommodate the sp-like occupied state (see Fig. 9), the unoccupied ground state, which prefers to occupy a more spherical cavity, is destabilized, leading to a large Stokes shift of ~2 eV. These same solvent motions that close the ground-to-first-excited-state energy gap also increase the gap between the occupied state and higher-lying excited states: The three sp-like excited states are quasidegenerate in the roughly spherical ground-state solvent cavity, but as the cavity becomes elongated to accommodate the (occupied) lowest of these states, the other two sp excited states that are oriented in orthogonal directions no longer "fit" as well in this cavity, so their energy is destabilized. Thus, the large gap to the ground state and the gap that opens between the occupied and higher-lying excited states leave little room for nonadiabatic coupling to mix any of the adiabatic eigenstates together.

In panel (b) of Figs. 6–8 we examine the Coulomb and exchange energies of the two electrons following excitation of aqueous 2EM sodide to the lowest CTTS state. We find that excitation instantaneously lowers the exchange energy relative to its ground-state value (cf. Table II). This can be understood in terms of the electronic structure of aqueous sodide: The ground state is ss-like and therefore both electrons largely occupy the same region of space, leading to exchange energy similar in magnitude to the Coulomb energy. The lowest CTTS excited state, in contrast, is largely sp-like and therefore the electrons are better able to avoid each other, leading to smaller exchange energy. As dynamic solvation of the excited state progresses, the Coulomb energy becomes smaller, indicating that the solvent is driving the electrons further apart, but the exchange energy stays roughly constant, indicating that the electrons maintain their degree of correlation.

The nature of how the solvent alters the electron-electron interaction in the CTTS state is further revealed in panel (c) of Figs. 6–8, which plot the total amount of charge Z that remains within 3.6 Å of the sodium cation core. Immediately following excitation, $Z \approx -0.6$, indicating that both electrons are mostly associated with the sodium core, although not as much as in the ground state (where $Z \approx -1$) since the excited state is more diffuse. As solvation proceeds, Z becomes closer to 0, reflecting the fact that only one of the two valence electrons is now associated with the sodium cation core because the other one has moved away into the liquid. This process can thus be considered a CTTS reaction: An initially electronically excited sodide ion reacts to form a neutral sodium atom and a solvated electron. Given that there is a nonzero exchange interaction between these species, the two electrons cannot be thought of as completely independent but rather should be treated as a single quantum mechanical object. We shall refer to this single quantum mechanical object as a sodium atom:electron contact pair.[21] Indeed, the ejected electron remains close to the sodium cation core, being ejected to a distance of ~5 Å, which is roughly the sum of the radii of a sodium atom and a hydrated electron. An examination of all of our trajectories (one of which is shown in Fig. 9) shows that the ejected electron occupies a solvent cavity immediately adjacent to the sodium atom without any intervening solvent molecules. Once the electron is ejected and the contact pair is formed, we see that fluctuations in E_{ex} and Z become larger; e.g., consider Fig. 6 for times between 100 and 769 fs and Fig. 8 for times between 100 and 195.5 fs. These fluctuations arise from solvent motions driving part of the ejected electron density back and forth between the original sodium solvent cavity and the cavity around the ejected electron.

To better visualize the solvation dynamics associated with CTTS excitation and the subsequent ejection of one electron and formation of the sodium atom:electron contact pair, in Fig. 9 we plot contours of the mean-field electronic density for the trajectory shown in Fig. 6. We see that excitation at $t=0$ creates an aspherical, peanut-shaped charge density with one lobe centered roughly on the sodium cation core and a smaller lobe pointing away from the cation. By 60 fs, the lobe that was pointing away from the cation has grown into a distinctive quasispherical ball of charge that is

only attached to the sodium atom by a thin tendril of charge; i.e., the sodium atom:electron contact pair has formed. In this trajectory, this species remains quasistable in the excited state until 796 fs when the transition to the ground state occurs, which we shall discuss in detail in Sec. IV A 2.

Perhaps the most remarkable result concerning the trajectories in Figs. 6–9 is that despite the substantial differences in electronic and solvent structure between the 1EM and 2EM simulations of sodide, the early-time behavior of the 2EM is similar to what was seen in the 1EM simulations. The 1EM nonadiabatic relaxation simulations all showed initial solvation that pushed the node of the p-like CTTS excited state away from the sodium core, the so-called "nodal migration."[46] This nodal migration in the 1EM simulations was driven by the water solvent trying to move into the node of the excited-state wave function since this region is depleted of electron density that had been present in the ground state. Because the solvent can only move into the node when the node is displaced from the relatively large 1EM neutral sodium core, the node of the excited wave function migrates such that one lobe of density overlaps the neutral core and the other extends into the solvent. In our 2EM simulations, we do not see nodes in the many-electron charge density, but we do see (cf. Fig. 9) that solvation produces an elongated excited-state electron density with a thin "neck" in the middle. Thus, it appears that the underlying solvation mechanism is the same: Water molecules move into this neck region, causing the ground state to destabilize and the electron density in the excited state to split into the sodium atom:electron contact pair.

Even though the basic CTTS mechanism is similar in both the 1EM and 2EM simulations of aqueous sodide, there is a significant difference in the rate at which the sodium atom:electron contact pair forms. In most of our 2EM trajectories, the CTTS ejection process is complete within 400 fs after excitation, and in some trajectories, such as the one shown in Figs. 6 and 9, contact-pair formation takes place as quickly as 60 fs. In the 1EM simulations, nodal migration took significantly longer than this: The solvent response was not complete until ~1 ps after excitation, and there were no trajectories in which the solvent response was complete before 400 fs. We believe that this difference results from the larger and less structured solvent cavity in the 2EM simulations relative to the 1EM: Because the original 2EM cavity is less structured, less reorganization is required to form the new cavity around the sodium atom:electron contact pair.

The faster solvation seen in the 2EM simulations is also reflected in the excited-state lifetime: In our 13 nonequilibrium 2EM trajectories, we found the average lifetime to be around 450 fs, with a shortest and longest lifetimes of 184.5 and 853.5 fs, respectively. We also found no clear difference in lifetimes between trajectories whose initial configurations fell into group 0, group 1, or group 2. In contrast, the average excited-state lifetime in the 1EM simulations was 1210 fs, and no trajectory returned to the ground state before 400 fs. Thus, the 1EM simulations substantially overestimate the excited-state lifetime of aqueous sodide. This may be in large part due to the differences in electronic structure of the two models, particularly since in the 1EM simulations, the sys-

tem had a much larger energy gap to close before the nonadiabatic transition to the ground state could occur.

2. Nonadiabatic transition to the ground state and subsequent relaxation dynamics of CTTS-excited aqueous sodide

Having seen that the initial dynamics following CTTS excitation of aqueous sodide is qualitatively the same in all of our 2EM nonequilibrium trajectories, we turn in this section to explore the differences that arise after the nonadiabatic transition to the ground state. After the nonadiabatic transition to the ground state, we see the dynamics follow one of two distinct pathways: Either the sodium atom:electron contact pair dissociates and the electron is detached, or the electron recombines with the sodium so that the contact pair collapses back into a ground-state sodium anion. None of our nonequilibrium trajectories showed the electron becoming completely free from the sodium atom, so we defined the electron as having detached when the exchange energy was less than 0.1 eV. With this definition, we found that 6 of our 13 nonequilibrium trajectories resulted in electron detachment. The experimental electron photodetachment quantum yield of sodide in weakly polar solvents, e.g., tetrahydrofuran (THF), is essentially unity,[25] so it appears that our choice of water as the solvent is what is responsible for the significant fraction of trajectories that undergo direct recombination. This is likely because it is energetically unfavorable to solvate a free neutral sodium atom in a highly polar solvent such as water. We will explore the nature of 2EM sodide's CTTS detachment dynamics in liquid THF in upcoming work.[87]

Figures 6 and 9 show the salient features of a representative detachment trajectory. The key features of the detachment process in this trajectory are seen in the 20 fs after transition to the ground state (at 760 fs, marked by the position of the arrow in Fig. 6): E_{ex} drops below 0.1 eV and Z increases to ~0, all of which indicate that the ejected electron has detached from the sodium atom and can be considered a separate chemical species. Once detachment occurs, we see large fluctuations in E_{ex} and Z, which reflect the fact that the solvent continues to drive some of the ejected electron density back and forth between the sodium and electron solvent cavities; presumably it is one of these fluctuations that eventually drives the electron completely back onto the sodium atom to reform the sodide anion, in this case, about 50 fs after the transition to the ground state. Across the six trajectories in which detachment occurred, we found that the electron remains detached in the ground state for times ranging from ~50 fs, the trajectory described above, up to ~500 fs, the trajectory shown in Fig. 8. In all cases, once detachment is complete, the separated sodium and electron eventually collapse to reform sodide, an event characterized by an increase in E_{ex} and a decrease in Z, and an opening of the ground- to excited-state energy gap.

Figure 7 shows a representative example of one of the seven nonequilibrium trajectories that followed a nondetachment pathway. In this trajectory and those like it, the sodium atom:electron contact pair begins to recombine immediately upon the transition to the ground state, as characterized by an

increase in E_{ex} and the CTTS energy gap, and a decrease in Z; in this case, the ground-state sodium anion is reformed in ~ 30 fs.

B. Effect of sodium cation solvation on the CTTS dynamics of aqueous sodide

The principal structural feature that we observed in the 2EM simulations that was absent in the 1EM simulations was the direct solvation of the sodium cation by water molecules. In this section, we analyze the effects of these solvating water molecules on the CTTS dynamics of excited 2EM sodide. The first thing we note is that of the seven trajectories that had initial configurations in which one or two water molecules solvated the cation (trajectories that were initially in group 1 or group 2), all seven maintained this solvation feature for at least the duration of the nonequilibrium response. In a few of the trajectories, the number of cation-solvating water molecules actually increased following CTTS excitation: Three trajectories that initially had $n_{Na^+}=0$ had one water molecule attach to the sodium cation at some point during the nonequilibrium dynamics, three trajectories that initially had $n_{Na^+}=1$ had $n_{Na^+}=2$ during the CTTS process, and one trajectory that initially had $n_{Na^+}=2$ reached $n_{Na^+}=4$. Thus, our nonstatistical selection of initial configurations shows that there is a greater preference for water molecules to solvate the sodium cationic core when sodide is in its CTTS excited state. This is presumably because the excited-state electron density lies further from the core than in the ground state, which allows water molecules to get closer to the cationic core. Although the presence of these solvating water molecules did not appear to have an appreciable influence on the excited-state lifetime, we did find that if cation-solvating waters were present during the transition to the ground state, then the trajectory was much more likely to undergo detachment. We interpret this as resulting from the fact that the presence of water molecules close to the cationic core destabilizes the sodide ground state, so that it is less likely that the excited sodium atom:electron contact pair can immediately recombine.

Figure 8 shows the results of one trajectory where the initial configuration had $n_{Na^+}=2$. In this trajectory, n_{Na^+} increases to 3 at $t=310$ and stays at that value until 1060 fs, when it drops back down to 2 (the system relaxes back to $n_{Na^+}=0$ after another ~ 500 fs, not shown). We see that the effect of this additional cation-solvating water is to further displace electron density away from the sodium cation, so that Z becomes greater than 0 and reaches ~ 0.1 at 680 fs. This observation is significant because it shows that the sodium atom that is left behind after detachment is polarized by the water in a similar manner to the sodide anion before excitation. This means that the physics associated with the cation solvation is missed by the 1EM, which cannot capture this behavior with its assumption that one of the two sodide valence electrons is chemically inert.

V. CONCLUSIONS

Using a many-electron simulation method, we have revisited the aqueous sodide system to understand how treat-

ment of electronic exchange and correlation affects MQC calculations of CTTS electronic structure and dynamics. We saw that the electronic structure of aqueous sodide calculated with our multielectron method was substantially different from that obtained with a 1EM.[46] First and foremost, the size of the sodium anion in the 2EM was significantly larger than in the 1EM. This size difference resulted in a larger and less ordered first solvation shell for 2EM aqueous sodide relative to the 1EM and led to an absorption spectrum for 2EM sodide that was 2 eV redshifted relative to the 1EM, in much better agreement with experiments in related solvents. In addition, the 1EM calculations predicted that the sodium anion has only three principal CTTS excited states, whereas our 2EM simulations showed that aqueous sodide has many bound excited states above the three principal CTTS states. These higher-lying bound states contribute to a blue tail in the absorption spectrum, similar to what is seen experimentally in other solvents.

Another important structural feature that the one-electron simulations could not properly capture is the propensity for water to induce large dipole moments in sodide. In water, the sodide anion has a large polarizability, $169a_0^3$, which cannot be correctly accounted for in a one-electron picture. With this polarizability, the fluctuating electric field from the nearby water molecules could induce instantaneous dipole moments of as large as 14 D. For the largest induced dipole moments, we also discovered an interesting solvation motif where the valence electrons are pushed so far off the sodium nucleus that the oxygen atom(s) of one (or two) nearby water molecule(s) can directly solvate the partially exposed sodium cation core. This type of close solvent approach could never be seen in one-electron simulations because the sodium core in the 1EM is neutral, not cationic. We also saw that the presence of these core-solvating water molecules played a role in electron detachment from the CTTS excited state of the multielectron anion; their absence in the 1EM raises serious questions about the meaning of CTTS dynamics calculated in the absence of an appropriate treatment of exchange and correlation. Finally, we saw that the use of a QM/MM-like approach, in which the more accurate electronic structure method was used with configurations generated from a lower-level calculation (2EM/1EC), led to a qualitatively accurate picture of the electronic structure but was quantitatively inaccurate. Moreover, the absence of a "quantum back reaction" would lead to an inaccurate prediction of the ion size and solvent structure, as well as miss features such as the direct solvation of the core.

Despite the substantial differences between the 1EM and 2EM, we found surprisingly that the 1EM did capture the basic nature of the principle CTTS states. The 2EM found that the principle CTTS states had sp angular character such that the shape of the charge density of the excited CTTS state was qualitatively similar in the 1EM and 2EM. We believe that this is the primary reason we saw qualitatively similar relaxation pathways in the 1EM and 2EM sodide nonequilibrium simulations, although we note that the 1EM simulations missed many of the important details and predicted relaxation time scales that were substantially too long.

Given the similarities in electronic structure between

aqueous sodide and the hydrated dielectron, as discussed in Sec. III, it is interesting to compare the nonequilibrium dynamics of the two species. In their studies of the hydrated dielectron, Larsen and Schwartz[55] simulated the nonequilibrium response following excitation to one of the high-lying excited states. These authors found that the excited dielectron cascaded nonadiabatically through the manifold of excited states to reach the lowest excited state in ≤100 fs. Once the dielectron reached this lowest excited state, the energy gap from this state to the ground state was ~2 eV, which is quite similar to that in our aqueous 2EM sodide. Thus, it makes sense to compare the nonequilibrium sodide trajectories discussed here to those from the previous dielectron work after the dielectron had relaxed to its lowest excited state.

In nonequilibrium simulations of the hydrated dielectron, Larsen and Schwartz[55] found that the lifetime of the dielectron in its first excited state was ~400 fs, which is quite similar to what we observe here for aqueous sodide. While in the lowest excited state, rearrangement of the solvent surrounding the dielectron caused the charge density to split into two lobes, which moved apart to a distance of about 5.5 Å. The resemblance of this relaxation motif to what we observe following CTTS excitation of 2EM sodide is striking: The only difference is that for the sodide system, one of the lobes of charge has a sodium cation in it. Overall, the nonequilibrium dynamics of sodide and the hydrated dielectron in their first excited state are very similar. We believe that this is a direct result of the similarities in the size and electronic structure of these two ions. Upon excitation, both of these ions change from a (roughly) spherical ground state with predominantly *ss* electronic symmetry to an elongated excited state with predominantly *sp* electronic symmetry. Thus, despite the facts that one of these ions has a nucleus and one does not and that one is singly charged and the other doubly charged, it is the similarity of the excited electronic charge density shape in these two systems that determines the similarity of the solvent response.

By focusing our efforts on the fictitious aqueous sodide system, we have been able to isolate the roles of exchange and correlation in the CTTS electronic structure and dynamics. The experimental ultrafast pump-probe studies of sodide's CTTS dynamics have all involved low-dielectric solvents, such as THF,[18–30,34,35] solvents which behave quite differently than water. In particular, it recently has become established that solvents such as THF are full of cavities that play an integral role in dictating the electronic structure and dynamics of solvent-supported excited states, such as CTTS states.[31,32,88–90] It is for this reason that we have not emphasized the connections between the calculations presented here and experiment; however, we are currently in the process of extending this work to perform multielectron simulations of sodide in THF.[87] Our preliminary results for the sodide/THF system suggest that our many-electron description of CTTS electronic structure will allow for direct contact with experiment and furnish a meaningful molecular interpretation of CTTS dynamics that has yet to be explored with an appropriate treatment of electronic exchange and correlation.

APPENDIX A: CONSTRUCTION OF A SMOOTH Na-ELECTRON PSEUDOPOTENTIAL

As mentioned in Sec. II B, the electron-water pseudopotential[48] we used in our simulations was developed using the PK theory.[50,51] Thus, to provide an internally consistent theoretical framework for our simulations, we require a PK pseudopotential for the sodium anion valence electrons within the FCHF approximation. To our knowledge, our group was the first to publish a fully rigorous PK sodium-electron pseudopotential.[64] However, we found that the sharply varying features in this pseudopotential (e.g., the features within 1 bohr of the sodium nucleus seen in Fig. 3 of Ref. [64]) rendered it inappropriate for use in molecular simulations: The features are so sharp that an extremely dense grid or other fine basis set would be required to represent wave functions that accurately sampled this pseudopotential. To proceed, we chose to smooth the PK pseudopotential in the core region, and this section describes our procedure for achieving this smoothing.

The goal of pseudopotential theory is to replace a multielectron Hamiltonian with a few-electron Hamiltonian, where the effect of most of the electrons is treated implicitly through the use of the pseudopotential. Typically, the minimum requirements of a pseudopotential are that it reproduces both the correct eigenvalue and the correct wave function of the explicitly treated electrons outside of the core region (where the implicitly treated electrons reside). PK theory rigorously meets these two requirements, although the resulting pseudopotential still has rapidly varying features in the core region. Thus, instead of using PK theory, we constructed a function, $\phi(r)$ (described below), that was smooth in the core region and which reproduced the Na atom's 3*s* valence electron FCHF wave function (i.e., the LUMO of the sodium cation) outside the sodium core. We then used this function to construct a pseudopotential by inverting a one-electron Schrödinger equation,[51]

$$V_p^{\text{local}}(r) = \frac{(\epsilon - \hat{T})\phi(r)}{\phi(r)}, \tag{A1}$$

where we set ϵ to be the Na atom 3*s* FCHF energy. This procedure yields a local sodium-electron pseudopotential, which strictly speaking should be used only to describe the sodium 3*s* state. The electron-water pseudopotential we used is also local, however, so that this sodium-electron pseudopotential provides the same level of description of the electronic structure. Thus, we felt that it was not necessary to construct and implement a more computationally expensive nonlocal sodium-electron pseudopotential.

The functional form we chose for $\phi(r)$ was a linear combination of Gaussian functions,

TABLE IV. Parameters used in the construction of the sodium-electron pseudopotential.

i	c_i (a.u.)	α_i (a.u.)
1	−0.103 055 903	0.189 844 564
2	0.436 627 83	0.069 933
3	0.541 733 81	0.032 893
4	0.134 538 22	0.016 122

$$\phi(r) = \sum_{i=1}^{4} c_i e^{-\alpha_i r^2}, \tag{A2}$$

whose coefficients c_i and α_i are listed in Table IV. These coefficients were chosen to provide the best fit to the Na 3s FCHF wave function and to ensure that the second derivative of $\phi(r)$ was zero at the origin; the latter condition is what ensured that our procedure led to a sufficiently smooth pseudopotential. Finally, because we chose Gaussians to represent the wave function used in constructing our pseudopotential, the long r asymptote of our pseudopotential was quadratic rather than following the correct $−1/r$ functional form.[64] We addressed this by tapering the calculated pseudopotential into a $−1/r$ function using a Steinhauser switching function;[59] we implemented the switch at 6 bohr over a 0.5 bohr range.

APPENDIX B: PROJECTION OF CI WAVE FUNCTIONS ONTO SPHERICAL HARMONICS

In this section, we derive the expressions we used to project our two-electron CI wave functions onto products of spherical harmonics. To perform these projections, we found it most convenient to rewrite the CI wave function, Ψ, in a basis of simple products of one-electron states, $\psi(\mathbf{r})$ (i.e., a basis without spin symmetry),

$$\Psi(\mathbf{r}_1, \mathbf{r}_2) = \sum_{i,j} \widetilde{c}_{ij} \psi_i(\mathbf{r}_1) \psi_j(\mathbf{r}_2). \tag{B1}$$

The double sum in Eq. (B1) runs over all N_{st} single-electron states, so that the size of the basis is N_{st}^2 [as opposed to $N_{st}(N_{st}-1)/2$ in the spin-singlet antisymmetrized basis]. We enforce spin-singlet symmetry by ensuring that the expansion coefficients obey $\widetilde{c}_{ij} = \widetilde{c}_{ji}$.

Once the CI wave function is represented in this basis, we proceed by expanding the $\psi(\mathbf{r})$ in terms of the spherical harmonics,

$$\psi_i(\mathbf{r}) = \sum_{l,m} C^i_{l,m}(r) Y_{l,m}(\Omega), \tag{B2}$$

where $Y_{l,m}$ is a spherical harmonic and $C^i_{l,m}$ is the expansion coefficient for single-electron state i,

$$C^i_{l,m}(r) = \int d\Omega \, Y^*_{l,m}(\Omega) \psi_i(\mathbf{r}), \tag{B3}$$

and Ω is the solid angle. Plugging Eq. (B2) into Eq. (B1) and rearranging allows us to derive the probability $P_{l,m,l',m'}$ to find electron 1 in angular momentum state $|l,m\rangle$ while electron 2 is in angular momentum state $|l',m'\rangle$,

$$P_{l,m,l',m'} = \int dr_1 r_1^2 \int dr_2 r_2^2 \left| \sum_{i,j} \widetilde{c}_{ij} C^i_{l,m}(r_1) C^j_{l',m'}(r_2) \right|^2. \tag{B4}$$

In principle, all we need to do is calculate all of the $C^i_{l,m}(r)$ using Eq. (B2), and then use Eq. (B4) and the CI coefficients to find the projections that we seek.

Direct implementation of this procedure, however, is somewhat problematic because the $\psi(\mathbf{r})$'s in our simulations are represented on a three-dimensional Cartesian grid, and transforming to polar coordinates would involve fitting the wave function between grid points. Thus, we follow Sheu and Rossky[4] and manipulate Eq. (B4) to allow all of the integrals to be done on the Cartesian grid. We begin by rewriting Eq. (B4) as

$$P_{l,m,l',m'} = \sum_{i,j} \sum_{k,l} \widetilde{c}_{ij} \widetilde{c}^*_{kl} p^{i,k}_{l,m} p^{j,l}_{l',m'}, \tag{B5}$$

where

$$p^{i,k}_{l,m} = \int dr \, r^2 C^i_{l,m}(r) C^k_{l,m}{}^*(r). \tag{B6}$$

The $p^{i,k}_{l,m}$ now resemble Eq. (A3) in Ref. 4, allowing us to use the trick of Sheu and Rossky of introducing an additional integration on r with a delta function and its Fourier representation. After some manipulation, we find

$$
\begin{aligned}
p^{i,k}_{l,m} = \frac{1}{\pi} \int_0^\infty dk & \left[\int d\tau \, Y^*_{l,m}(\Omega) \psi_i(\mathbf{r}) \frac{\cos(kr)}{r} \right] \\
& \times \left[\int d\tau \, Y_{l,m}(\Omega) \psi_k^*(\mathbf{r}) \frac{\cos(kr)}{r} \right] \\
& + \left[\int d\tau \, Y^*_{l,m}(\Omega) \psi_i(\mathbf{r}) \frac{\sin(kr)}{r} \right] \\
& \times \left[\int d\tau \, Y_{l,m}(\Omega) \psi_k^*(\mathbf{r}) \frac{\sin(kr)}{r} \right],
\end{aligned} \tag{B7}
$$

where the integrals involving the single-electron states are now performed over all space ($d\tau$) and therefore can be evaluated on the Cartesian grid. The compromise in using Eq. (B7) is the introduction of an additional integral on k, which we evaluated numerically. Since our single-electron states are represented on a regular real-space grid with grid spacing d, our k integrals are evaluated only up to the largest k component the grid can support, $k = \pi/(2d)$.

Finally, in order to calculate the probability of finding one electron in angular momentum state l while the other is in state l' (as shown in Table III), we added $P_{l,m,l',m'}$ and $P_{l',m',l,m}$ (for $l \neq l'$) and summed over m and m'.

[1] M. Smith and M. C. R. Symons, Trans. Faraday Soc. **54**, 338 (1958).
[2] J. Jortner, M. Ottolenghi, and G. Stein, J. Phys. Chem. **68**, 247 (1964).
[3] M. J. Blandamer and M. F. Fox, Chem. Rev. (Washington, D.C.) **70**, 59 (1970).
[4] W. S. Sheu and P. J. Rossky, J. Phys. Chem. **100**, 1295 (1996).
[5] Y. Gauduel, H. Gelabert, and M. Ashokkumar, Chem. Phys. **197**, 167 (1995).
[6] J. A. Kloepfer, V. H. Vilchiz, V. A. Lenchenkov, and S. E. Bradforth, Chem. Phys. Lett. **298**, 120 (1998).
[7] F. H. Long, H. Lu, X. Shi, and K. B. Eisenthal, Chem. Phys. Lett. **169**,

165 (1990).

[8] F. H. Long, X. L. Shi, H. Lu, and K. B. Eisenthal, J. Phys. Chem. **98**, 7252 (1994).

[9] J. A. Kloepfer, V. H. Vilchiz, V. A. Lenchenkov, A. C. Germaine, and S. E. Bradforth, J. Chem. Phys. **113**, 6288 (2000).

[10] V. H. Vilchiz, J. A. Kloepfer, A. C. Germaine, V. A. Lenchenkov, and S. E. Bradforth, J. Phys. Chem. A **105**, 1711 (2001).

[11] J. A. Kloepfer, V. H. Vilchiz, V. A. Lenchenkov, X. Y. Chen, and S. E. Bradforth, J. Chem. Phys. **117**, 766 (2002).

[12] M. C. Sauer, I. A. Shkrob, R. Lian, R. A. Crowell, D. M. Bartels, X. Y. Chen, D. Suffern, and S. E. Bradforth, J. Phys. Chem. A **108**, 10414 (2004).

[13] V. H. Vilchiz, X. Chen, J. A. Kloepfer, and S. E. Bradforth, Radiat. Phys. Chem. **72**, 159 (2005).

[14] R. Lian, D. A. Oulianov, R. A. Crowell, I. A. Shkrob, X. Y. Chen, and S. E. Bradforth, J. Phys. Chem. A **110**, 9071 (2006).

[15] A. C. Moskun, S. Bradforth, J. Thogersen, and S. Keiding, J. Phys. Chem. A **110**, 10947 (2006).

[16] X. Chen and S. Bradforth, Annu. Rev. Phys. Chem. **59**, 203 (2008).

[17] M. C. Sauer, R. A. Crowell, and I. A. Shkrob, J. Phys. Chem. A **108**, 5490 (2004).

[18] E. R. Barthel, I. Martini, and B. J. Schwartz, J. Chem. Phys. **112**, 9433 (2000).

[19] I. B. Martini, E. R. Barthel, and B. J. Schwartz, J. Chem. Phys. **113**, 11245 (2000).

[20] I. B. Martini, E. R. Barthel, and B. J. Schwartz, Science **293**, 462 (2001).

[21] E. R. Barthel, I. Martini, and B. J. Schwartz, J. Phys. Chem. B **105**, 12230 (2001).

[22] I. B. Martini, E. R. Barthel, and B. J. Schwartz, J. Am. Chem. Soc. **124**, 7622 (2002).

[23] I. B. Martini and B. J. Schwartz, Chem. Phys. Lett. **360**, 22 (2002).

[24] E. R. Barthel, I. B. Martini, E. Keszei, and B. J. Schwartz, J. Chem. Phys. **118**, 5916 (2003).

[25] E. R. Barthel and B. J. Schwartz, Chem. Phys. Lett. **375**, 435 (2003).

[26] E. R. Barthel, I. B. Martini, E. Keszei, and B. J. Schwartz, in *Ultrafast Phenomena XIII*, edited by M. Murnane, N. Scherer, R. J. D. Miller, and A. M. Weiner (Springer-Verlag, Berlin, 2003), pp. 459–461.

[27] I. B. Martini, E. R. Barthel, and B. J. Schwartz, in *Ultrafast Phenomena XIII*, edited by M. Murnane, N. Scherer, R. J. D. Miller, and A. M. Weiner (Springer-Verlag, Berlin, 2003), pp. 487–489.

[28] I. B. Martini and B. J. Schwartz, J. Chem. Phys. **121**, 374 (2004).

[29] I. B. Martini, E. R. Barthel, and B. J. Schwartz, Pure Appl. Chem. **76**, 1809 (2004).

[30] M. C. Cavanagh, R. E. Larsen, and B. J. Schwartz, J. Phys. Chem. A **111**, 5144 (2007).

[31] A. E. Bragg and B. J. Schwartz, J. Phys. Chem. B **112**, 483 (2008).

[32] A. E. Bragg and B. J. Schwartz, J. Phys. Chem. A **112**, 3530 (2008).

[33] M. C. Cavanagh, R. M. Young, and B. J. Schwartz, J. Chem. Phys. **129**, 134503 (2008).

[34] Z. H. Wang, O. Shoshana, B. X. Hou, and S. Ruhman, J. Phys. Chem. A **107**, 3009 (2003).

[35] O. Shoshana, J. L. P. Lustres, N. P. Ernsting, and S. Ruhman, Phys. Chem. Chem. Phys. **8**, 2599 (2006).

[36] O. Shoshanim and S. Ruhman, J. Chem. Phys. **129**, 044502 (2008).

[37] H. Iglev, R. Laenen, and A. Laubereau, Chem. Phys. Lett. **389**, 427 (2004).

[38] H. Iglev, A. Trifonov, A. Thaller, I. Buchvarov, T. Fiebig, and A. Laubereau, Chem. Phys. Lett. **403**, 198 (2005).

[39] W. S. Sheu and P. J. Rossky, Chem. Phys. Lett. **202**, 186 (1993).

[40] W. S. Sheu and P. J. Rossky, Chem. Phys. Lett. **213**, 233 (1993).

[41] W. S. Sheu and P. J. Rossky, J. Am. Chem. Soc. **115**, 7729 (1993).

[42] D. Borgis and A. Staib, Chem. Phys. Lett. **230**, 405 (1994).

[43] A. Staib and D. Borgis, J. Chem. Phys. **104**, 9027 (1996).

[44] D. Borgis and A. Staib, J. Chem. Phys. **104**, 4776 (1996).

[45] D. Borgis and A. Staib, J. Phys.: Condens. Matter **8**, 9389 (1996).

[46] C. J. Smallwood, W. B. Bosma, R. E. Larsen, and B. J. Schwartz, J. Chem. Phys. **119**, 11263 (2003).

[47] S. E. Bradforth and P. Jungwirth, J. Phys. Chem. A **106**, 1286 (2002).

[48] J. Schnitker and P. J. Rossky, J. Chem. Phys. **86**, 3462 (1987).

[49] F. Webster, P. J. Rossky, and R. A. Friesner, Comput. Phys. Commun. **63**, 494 (1991).

[50] J. C. Phillips and L. Kleinman, Phys. Rev. **116**, 287 (1959).

[51] L. Szasz, *Pseudopotential Theory of Atoms and Molecules* (Wiley, New York, 1985).

[52] R. E. Larsen and B. J. Schwartz, J. Chem. Phys. **119**, 7672 (2003).

[53] R. E. Larsen and B. J. Schwartz, J. Phys. Chem. B **108**, 11760 (2004).

[54] R. E. Larsen and B. J. Schwartz, J. Phys. Chem. B **110**, 1006 (2006).

[55] R. E. Larsen and B. J. Schwartz, J. Phys. Chem. B **110**, 9681 (2006).

[56] R. E. Larsen and B. J. Schwartz, J. Phys. Chem. B **110**, 9692 (2006).

[57] K. Toukan and A. Rahman, Phys. Rev. B **31**, 2643 (1985).

[58] P. B. Balbuena, K. P. Johnston, and P. J. Rossky, J. Phys. Chem. **100**, 2706 (1996).

[59] O. Steinhauser, Mol. Phys. **45**, 335 (1982).

[60] The errors associated with truncating the long-range Coulomb interactions in our simulation were somewhat reduced by adopting a group-based cutoff scheme so that the longest ranged interactions were charge-dipole interactions. Although there exist better methods to treat long-range interactions in MD simulations, e.g., the Ewald summation (Ref. 61) we decided to use this simpler cutoff approach to allow for direct comparison to the 1EM sodide (Ref. 46) and dielectron simulations (Ref. 52), which also used the simple truncation scheme.

[61] M. P. Allen and D. J. Tidlesley, *Computer Simulation of Liquids* (Oxford University Press, London, 1992).

[62] P. Pulay, in *Applications of Electronic Structure Theory*, edited by H. F. Schaefer III (Plenum, New York, 1977).

[63] O. V. Prezhdo and P. J. Rossky, J. Chem. Phys. **107**, 825 (1997).

[64] C. Smallwood, R. E. Larsen, W. J. Glover, and B. J. Schwartz, J. Chem. Phys. **125**, 074102 (2006).

[65] The experimental electron affinity of a sodium cation is 0.188 857 6 hartree [*CRC Handbook of Chemistry and Physics*, 88th ed., edited by D. R. Lide (CRC/Taylor and Francis, Boca Raton, 2008)] the difference between this value and the negative of the frozen-core HF eigenvalue is due mainly to electron correlation between the valence and core electrons being neglected in the frozen core approximation [see W. Müller, J. Flesch, and W. Meyer, J. Chem. Phys. **80**, 3297 (1984)].

[66] W. C. Martin and R. Zalubas, J. Phys. Chem. Ref. Data **10**, 153 (1981).

[67] H. Hotop and W. C. Lineberger, J. Phys. Chem. Ref. Data **14**, 731 (1985)].

[68] The reason for our choice of single-electron adiabatic states over other possible bases, e.g., HF orbitals, is that these adiabatic states are easy to generate by diagonalizing a one-electron Hamiltonian: No self-consistent iterations are required. Furthermore, the excited-state HF orbitals (virtuals) are often unbound and are thus a poor representation of the lowest-lying many-electron excited-state wave functions, so that a large number of these states are required to form an adequate product basis. Our choice of the single-electron adiabatic product basis gives many bound higher-lying basis states, providing greater flexibility to simultaneously represent both the many-electron ground and lowest excited states.

[69] The mean potential energy of the dielectron-water interaction was calculated from the mean values of the dielectron total and kinetic energy and the electron-electron interaction energy as reported in Ref. 53, which is why the uncertainty in this value is unknown.

[70] We note that the lower states also could have substantial many-electron character in the form of radial correlation, although we have not probed this in our analysis.

[71] A gas-phase calculation of sodide's electronic structure with our two-electron model reveals that the ground state has 9% pp character.

[72] W. A. Seddon, J. W. Fletcher, and F. C. Sopchyshyn, Can. J. Chem. **54**, 3672 (1976).

[73] W. A. Seddon, J. W. Fletcher, F. C. Sopchyshyn, and E. B. Selkirk, Can. J. Chem. **57**, 1792 (1979).

[74] J. Heuft and E. Meijer, J. Chem. Phys. **119**, 11788 (2003).

[75] J. Heuft and E. Meijer, J. Chem. Phys. **122**, 094501 (2005).

[76] J. Heuft and E. Meijer, J. Chem. Phys. **123**, 094506 (2005).

[77] L. Dang, J. Rice, J. Caldwell, and P. Kollman, J. Am. Chem. Soc. **113**, 2481 (1991).

[78] K. Hashimoto, T. Kamimoto, and K. Daioku, J. Phys. Chem. A **104**, 3299 (2000).

[79] The dipole moment of a charged species depends on the origin of the coordinate system, which for sodide we took to be r_{Na^+}.

[80] D. Logan, Phys. Rev. Lett. **57**, 782 (1986).

[81] V. Dobrosavljevic, C. Henebry, and R. Stratt, J. Chem. Phys. **91**, 2470 (1989).

[82] N. C. Pyper and P. P. Edwards, J. Am. Chem. Soc. **122**, 5092 (2000).

[83] L. D. Landau and E. M. Lifshitz, *Quantum Mechanics*, 3rd ed. (Pergamon, New York, 1991).

[84] An empirical estimate of the solution-phase polarizability of sodide has been previously reported as $430a_0^3$ by Pyper and Edwards (Ref. 82). This

estimate is considerably larger than our calculated polarizability of $169 \pm 4 a_0^3$, and is based on the assumption that changes in sodide's polarizability between different phases are the same as for the iodide ion. We believe that this assumption is not valid given the very different electronic structure of iodide and sodide.

[85] C. Lupinetti and A. Thakkar, J. Chem. Phys. **125**, 194317 (2006).

[86] We chose to integrate the charge density up to 3.6 Å since we found empirically that this gave the most contrast between instances when both electrons were attached to the sodium core ($Z \approx -1$) and when one electron was detached ($Z \approx 0$).

[87] W. J. Glover and B. J. Schwartz (unpublished).

[88] M. J. Bedard-Hearn, R. E. Larsen, and B. J. Schwartz, J. Chem. Phys. **122**, 134506 (2005).

[89] M. J. Bedard-Hearn, R. E. Larsen, and B. J. Schwartz, J. Chem. Phys. **125**, 194509 (2006).

[90] D. T. Bowron, J. L. Finney, and A. K. Soper, J. Am. Chem. Soc. **128**, 5119 (2006).

[91] The standard deviations in Table II were calculated by computing the root-mean-square deviation and dividing by the square root of the number of independent samples, which was taken to be the length of the run divided by the estimated decorrelation time of the listed property (roughly 0.2 ps).